UNIVERSITY OF CALIFORNIA,
IRVINE

Spatial-temporal dynamics and metabolic alterations of p53 upon cellular stress

THESIS

submitted in partial satisfaction of the requirements
for the degree of

MASTER OF SCIENCE

in Biomedical Engineering

by

Swathi S Bagilthaya

Thesis Committee:
Assistant Professor Michelle Digman, Chair
Professor Enrico Gratton
Professor Lee Bardwell

2015

DEDICATION

To

my grandfather

who believed that there is no greater power than knowledge and would have been extremely proud of me

TABLE OF CONTENTS

LIST OF FIGURES

Page

ACKNOWLEDGMENTS

I would like to express my sincere gratitude towards my Committee chair and Principal Investigator, Dr. Michelle Digman for guiding me through the entire process with patience and persistence. I'm extremely grateful to have been given this opportunity to work for such an amazing project. Having come from a biology background with no previous experience with fluorescence microscopy, it was overwhelming at first but her unwavering encouragement motivated me to challenge myself and achieve my goals.

I would like to thank both my committee members, Dr. Enrico Gratton and Dr. Lee Bardwell. Dr. Gratton for generously allowing me to use all the facilities in the Laboratory for Fluorescence Dynamics (LFD) without which my research would've certainly been a nightmare if not impossible. Second, Dr. Lee Bardwell for providing the p53 mutants crucial for my experiments and for his insightful suggestions that helped in shaping up my thesis.

I'd also like to say thank you to all the LFD and Digman lab members, especially Milka Stakic for helping me with my cell cultures, Michael Murata for taking the time to assist me with my data analysis and Ramon Roca since misery really does love company.

Finally, I'd like to thank my parents, Subramanya and Shobha Bagilthaya for their unconditional support and faith throughout this journey that helped me overcome my obstacles and of course, my friends who kept me sane during the hard times.

ABSTRACT OF THE THESIS

Spatial-temporal dynamics and metabolic alterations of p53 upon cellular stress

By

Swathi Bagilthaya

Master of Science in Biomedical Engineering

University of California, Irvine, 2015

Assistant Professor Michelle Digman, Chair

p53 is a tumor suppressor protein that plays a very important role in determining the fate of damaged cells. Depending on the extent of damage, p53 being a transcription factor, induces target genes that are involved in cell repair mechanisms and apoptosis. In doing so, it prevents proliferation of abnormal cells that could lead to tumorigenesis. Primarily existing in its monomeric or dimeric form, when activated, it binds to DNA as a tetramer. The localization of these tetramers in cells has never been mapped. Since p53 is mutated in 50% of human cancers, its ability to tetramerize efficiently and hence bind to the DNA is disrupted leading to tumor progression. Here we use the Number and Brightness (N&B) analysis, a powerful method to measure protein oligomerization pixel by pixel from raster scanned images thereby providing spatial maps of p53 aggregates. The research described here shows, for the first time, the oligomerization maps of the p53 protein and its mutant counterparts to establish the crucial role of p53 tetramers in tumor suppression. In addition, p53 also regulates the metabolism of the cell by modulating important metabolic pathways upon cellular stress. To determine whether this switch is indicative of the balance between apoptosis and DNA repair, the phasor approach to lifetime imaging microscopy (FLIM) was employed to detect the free and bound lifetime of reduced nicotinamide adenine dinucleotide (NADH). The shifts in lifetime are informative of the

level of stress and give an indication whether the cell is undergoing cell cycle arrest or apoptosis. The ratios of free and bound NADH obtained from this data may be used as a marker of transcriptional activity. The N&B and FLIM results together provide an insight to p53 activation and this information can be further exploited to improve the field of cancer research.

CHAPTER 1

Introduction

The p53 protein, encoded by the TP53 gene, is a tumor suppressor protein and is crucial in regulating the cell cycle in multicellular organisms. It has been described as the 'Guardian of the genome', due to its role in conserving stability and preventing genome mutations[1]. p53 is mutated in 50% of human cancers and is therefore one of the most studied proteins. In addition, many of the tumors that do not exhibit the p53 mutation contribute to its inactivation by mutating genes involved in p53 regulation. Due to its vital role in cancer, it is a favourable target for developing therapeutic strategies and any breakthrough in this field of research may have clinical implications in the near future.

1.1 p53 and its many functions

p53 functions as a DNA-binding transcription factor and is activated in response to a wide variety of cellular stressors such as DNA damage, osmotic stress, ribosome dysfunction, hypoxia, nutrient deprivation and oncogene activation[2]. On activation, it regulates target genes involved in cell cycle arrest, DNA repair and/or apoptosis[3]. The dual function of p53 in inducing either damage mitigation and repair or apoptosis depends on the physiological circumstances and cell type. When exposed to low or moderate levels of stress, the subtle behaviour of p53 can play a role in the protection and survival of the cells by activating transcription of proteins involved in repair. It can arrest the growth by holding the cell cycle at the G1/S regulation point and

allowing the DNA repair proteins to fix the damage. The growth arrest stops the progression of cell cycle, preventing the replication of damaged DNA. In the presence of high stress, p53 activates transcription of proteins involved in apoptosis that would irreversibly remove the cells from the proliferating cycle. This is the last resort and usually the case when DNA damage is irreparable.

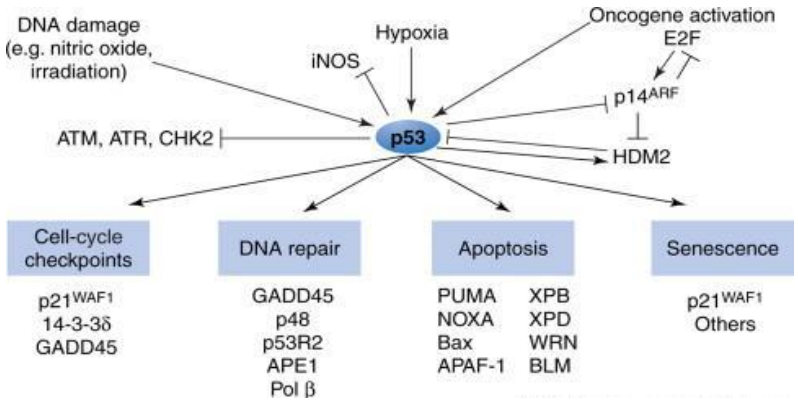

Fig. 1.1: p53 regulation of various target genes involved in different stress responsive functions [4]

Under unstressed conditions, p53 exists primarily in a monomeric or dimeric state or as a mixture of both monomers and dimers. However, when activated upon stress, p53 is known to exist as a tetramer[5].The tetramerization of p53 is a requirement for formation of a stable p53–DNA complex and is sufficient to induce the subsequent transactivation of target genes[6]. Since p53 tetramers have a much higher DNA binding affinity than p53 dimers, p53 must exist as a tetramer in its active form [7], as shown in fig. 1.2.

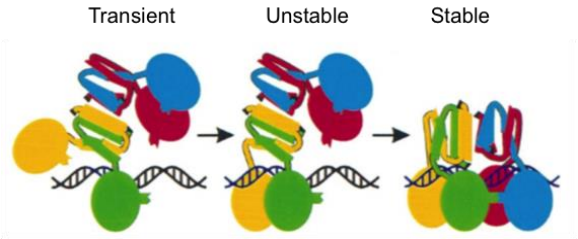

Fig. 1.2: Stability of p53 tetramer complex with DNA[7]

The spatiotemporal localization of these tetramers has never been mapped in a living cell and may provide an insight to study p53 activation and manipulate them at an appropriate time scale.

1.2 Regulation of p53

p53 is negatively regulated by the Mdm2 protein[8–10]. p53 and Mdm2 function in a negative feedback loop, with p53 driving the transcription of Mdm2 during times of normal homeostasis and Mdm2 in turn, maintaining low levels of p53 through a process of continuous degradation. In unstressed cells, Mdm2 induces the degradation of p53 by covalently attaching ubiquitin as seen in fig. 1.3, hence preventing the action of p53. In response to stress, p53 ubiquitination is inhibited resulting in a high level of p53 accumulation and in turn triggers the formation of p53 tetramers[11].

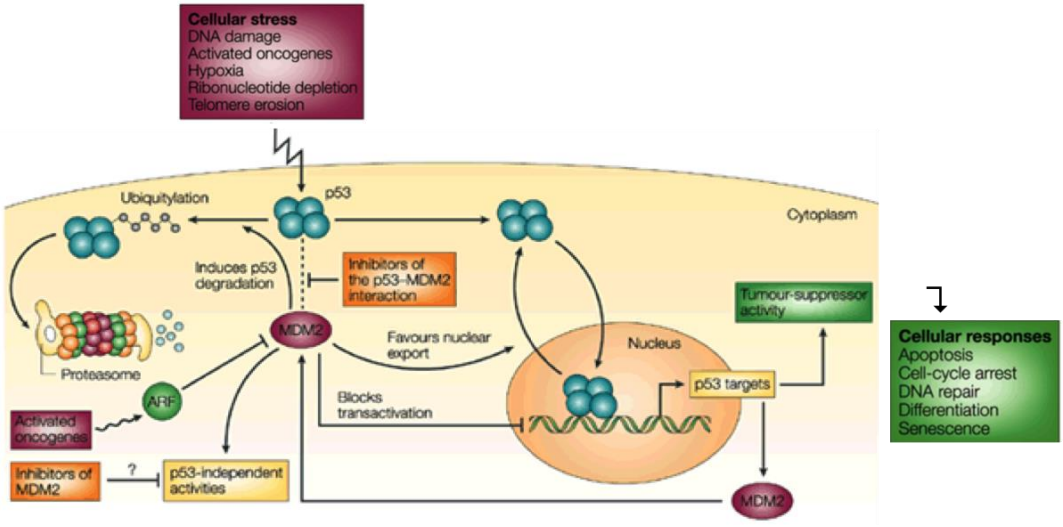

Fig. 1.3: Role of p53 in tumor suppression as a response to cellular stress. Fig. also shows the regulation of p53 by Mdm2[12]

1.3 Structure of p53

p53 exhibits a molecular mass of 53 kDa, comprising of 393 amino acids[13]. It has a modular domain structure consisting of folded tetramerization and DNA binding domains interspersed by disorganized regions at the amino- and carboxy- termini. Fig. 1.4 shows the domain structure of p53 (top panel). The structure is composed of five domains: a natively unfolded N-terminal transactivation domain (TAD) that allows p53 to activate other genes after binding to their regulatory regions; a proline rich domain; a central site specific DNA binding domain (fig. 1.4, bottom panel); a tetramerization/oligomerization domain (TD/OD) and a regulatory domain (CTD), similar to the TAD, disordered at the C-terminal. The DNA binding domain and the tetramerization domains are the main areas of interest as these are the regions housing mutations that give rise to cancer as shown in fig. 1.5.

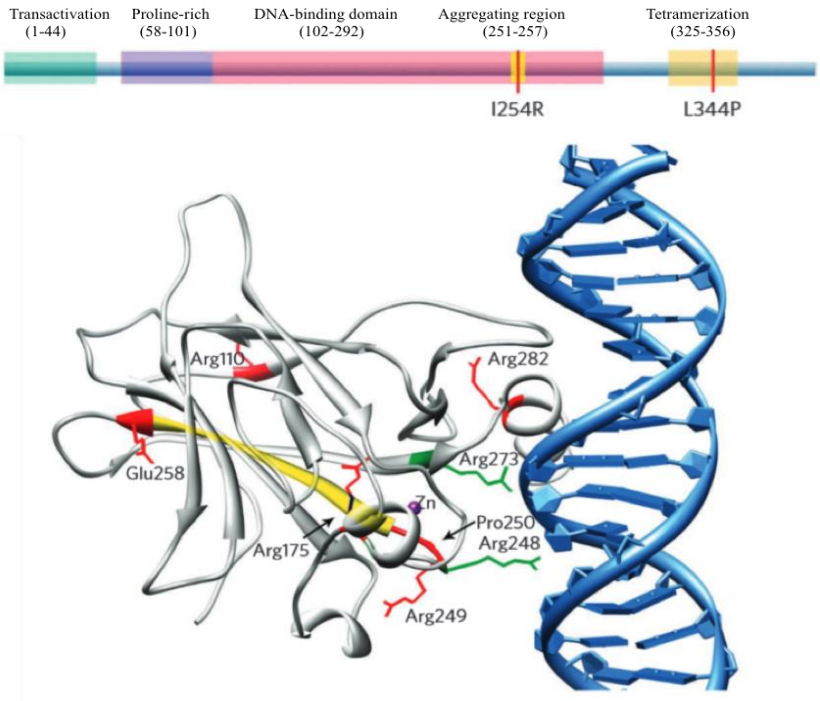

Fig 1.4: (a) Domain structure of P53 (b) DNA binding locations in the DNA binding domain[14]

More than 50 percent of human tumors contain a mutation or deletion of the p53 gene[15–17]. The mutant cells lack functional p53 as a result of which they cannot undergo cell cycle arrest or apoptosis in response to carcinogenic stress or oncogene activation. The primary alteration contributing to p53 mutations is a single amino acid substitution that seems modest in a 393 amino acid protein [18]. These cluster primarily at the DNA binding domain, contributing to a number of hotspot mutations (R175H, R248Q, R273S etc.). In addition, mutations also occur in the tetramerization domain despite its short amino-acid sequence; although at a very low frequency (4%)[19]. Germline mutations in this domain have been identified in patients with Li-Fraumeni and Li-Fraumeni like syndromes [20]. More about these mutations will be discussed in detail further in this chapter.

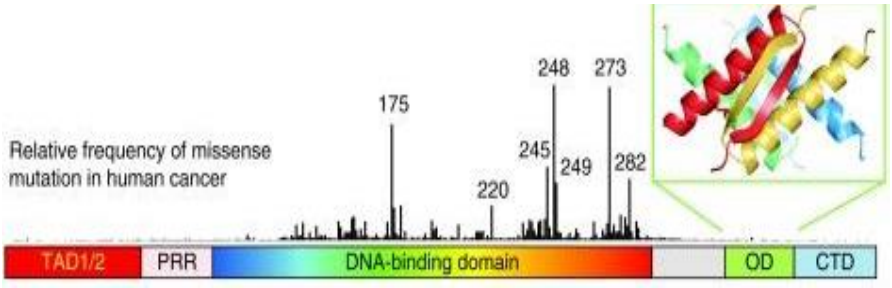

Fig 1.5: Occurrence of hot spot mutations in the DNA binding domain[15]

Recently, there has been tremendous research in this area to develop therapies and drugs that strive to restore the wild type function in p53 mutations [21]. A thorough understanding of the mechanism of wild-type p53 in comparison with its mutant counterparts may provide an insight to combat tumor progression.

1.4 Measuring p53 tetramerization with Number and Molecular Brightness (N&B) method

The N&B analysis is a statistical fluorescence fluctuation method of determining the protein concentration and aggregation state in cells[22]. The N&B has an advantage over existing methods such as the photon counting histogram analysis (PCH) and fluorescence intensity distribution analysis (FIDA) that can provide information about molecular aggregates only in a small focal volume. The N&B method provides a single pixel resolution map of molecular aggregates by calculating the number and molecular brightness at each pixel and with this information, the oligomerization state of the protein can be determined.

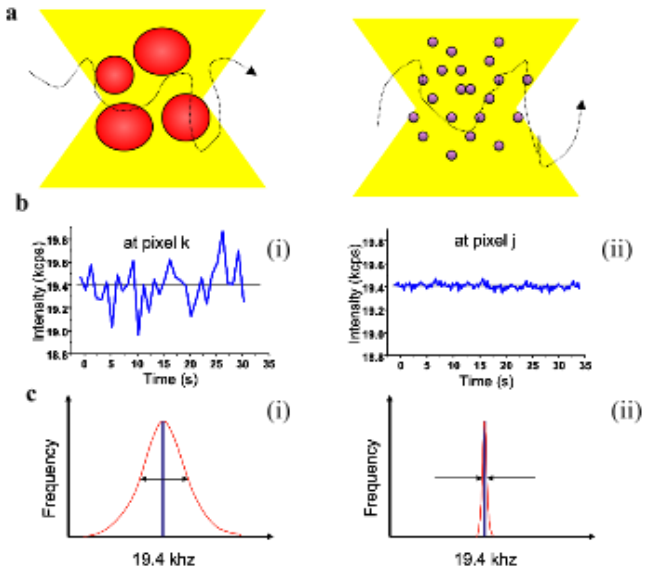

Fig. 1.6: (a) Observation volume consisting of (i) tetramers (ii) monomers; (b)Fluctuations in intensity with respect to time where the average intensity is the same at pixel k and j although a larger variance in intensity is exhibited by (i)compared to (ii); (c) Shows the histogram of counts corresponding to (b)

In the N&B method, the first (average intensity) and second (variance) moment of the intensity distribution are calculated. Fig. 1.6(a) depicts two pixels with the same average intensity but considerable difference in variance of the fluctuation of molecules within that volume. Since the tetramers are larger and brighter, the movement of these molecules in and out will generate

larger fluctuations. Therefore, even though the average intensities are the same, the variance in intensity is much larger in this case as compared with that of the monomers

By calculating the average intensity and variance in each pixel in a time series of images, the apparent brightness and average number of molecules can be estimated.

Average intensity (first moment), $< k >= \frac{\sum_i k_i}{K}$ (1)

Variance (second moment), $\sigma^2 = \frac{\sum_i (k_i - <k>)^2}{K}$ (2)

Apparent number of molecules, $< N >= \frac{<k>^2}{\sigma^2}$ (3)

Apparent molecular brightness, $B = \frac{<k>}{<N>} = \frac{\sigma^2}{<k>}$ (4)

where, <k> is the average counts, B is the apparent molecular brightness, N is the apparent number of molecules and σ^2 is the variance.

The variance due to the particles fluctuating in the observation volume is proportional to the square of the particle brightness and will have a B>1. The variance of the immobile fraction, the autofluorescence and that of the detector is proportional to the intensity of these components and in this case, B=1. B is related to the true molecular brightness, ε, of the particles and it is independent on the number of particles. In general, B cannot be obtained by the simple calibration procedure based on the intensity of a solution of known concentration. N is directly proportional to the number of particles n. It is very easy to extract n and ε from the above equations. In our imaging setup, we use an analog detector and the shot noise from these detector give rise to variance in our calculations. Thus, we must account for the variance from the detector shot noise which is directly proportional to the product of the true molecular brightness (ε) and the true number of molecules (n).

$$\sigma^2 = \sigma_d^2 + \sigma_n^2 \quad (5)$$

$$\sigma_n^2 = \varepsilon^2 n \quad (6)$$

$$\sigma_d^2 = \varepsilon\, n \quad (7)$$

$$\langle k \rangle = \varepsilon\, n \quad (8)$$

where, σ_n^2 is the variance due to occupation number, σ_d^2 variance due to detector shot noise, ε is the molecular brightness and *n* is the average number of molecules in the illumination volume.

Therefore, with this analysis, it is possible to map the spatial localization of the p53 oligomers in cells at real time.

1.5 Stress inducing agents

The oligomerization of p53 was induced by subjecting the cells to different modes of stress such as ribotoxic stress, DNA damage and environmental stress introduced in the form of the reagents anisomycin, cisplatin and sodium chloride solution respectively.

Anisomycin, (2-*p*-methoxyphenylmethyl-3-acetoxy-4-hydroxypyrrolidine), is a bacterial antibiotic that inhibits protein synthesis by binding to the 60s ribosomal subunit and blocking peptide bond formation[23]. Partial inhibition of DNA synthesis is observed at anisomycin concentrations that affect 95% inhibition of protein synthesis.

Cisplatin, or cis-diamminedichloroplatinum (II), is a chemotherapeutic drug and functions by damaging the DNA[24]. It forms a platinum complex inside the cell that binds to and crosslinks DNA, thereby blocking replication and transcription [25]

It is known that mammalian cells activate p53 in response to genotoxic or environmental stress. Mdm2[26] is down regulated in treatment with hypoxia as a result of which there is an

accumulation of p53[27]. Osmotic shock treatment was induced with a solution of 130mM NaCl to stimulate p53 accumulation.

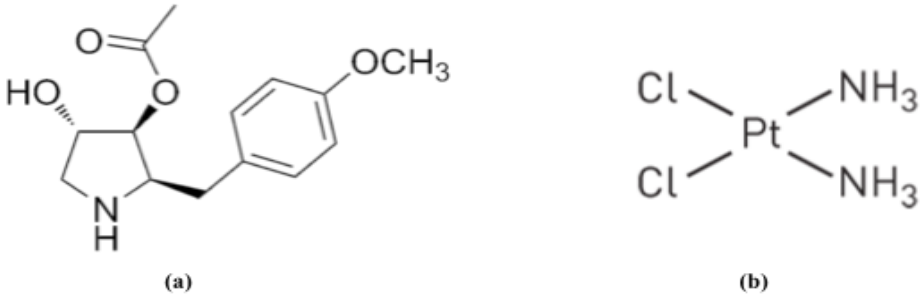

Fig. 1.7: (a) Structure of anisomycin (b) Structure of cisplatin

1.6 p53 mutations

Five mutant alleles of p53-GFP were constructed with three having mutations in the sequence specific DNA domain and the other two exhibiting mutations in the tetramerization domain. Those exhibiting mutations in the tetramerization domain, L344P &L344A, are theoretically expected to prevent oligomerization.

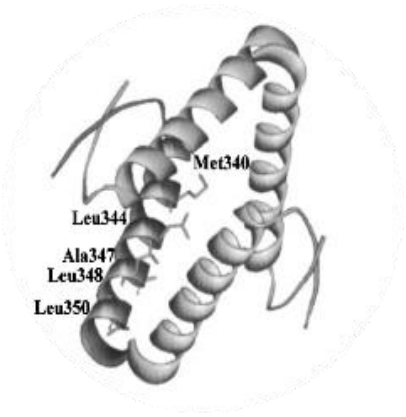

Fig 1.8: Four chains of the TD in a tetramer are represented. The amino acid residues involved in complex formation are shown for one chain[19]

As shown in fig. 1.8, Leu344, Ala347, Leu348, Leu350 and Met 340 residues constitute the hydrophobic core of the p53 tetramerization domain and are crucial for tetramerization[19]. The hydrophobic force is essential for stabilizing the domain and a mutation in any one of these residues could therefore disturb this balance. The mutants, L344A and L344P, were therefore used for these experiments and would reveal the effect of a single amino acid substitution in the TD on the p53 stability. Although, in vitro analysis and cellular assays of alanine mutations reveal the prevention of tetramerization and inactivation of the protein, it was uncertain of the effects in vivo. Many reports have shown the p53 variants in which the TD has been deleted are still able to bind to the DNA and enable transcription since the p53 monomers bind to DNA in a cooperative manner[6]. The DNA binding affinity however is 10-100 times lower than the full length protein. Another hypothesis is that the TD is particularly resistant to mutations and more than one mutation is required to destabilize it. The activity of these mutants may also depend on the level of expression i.e. they are inactive at low levels and can be activated at a higher level of expression. Since, most of the analyses have been in vitro studies so far, it would be interesting to observe the dynamics of these mutated proteins in vivo and assess whether all the above factors played any role whatsoever.

Unlike, the TD mutations that lead to a loss of p53 tumor suppressor activity, the DBD mutations exhibit a gain of function that promotes tumorigenicity[16]. This is one of the main reasons that they are assumed to appear more frequently in cancer compared to TD mutations.

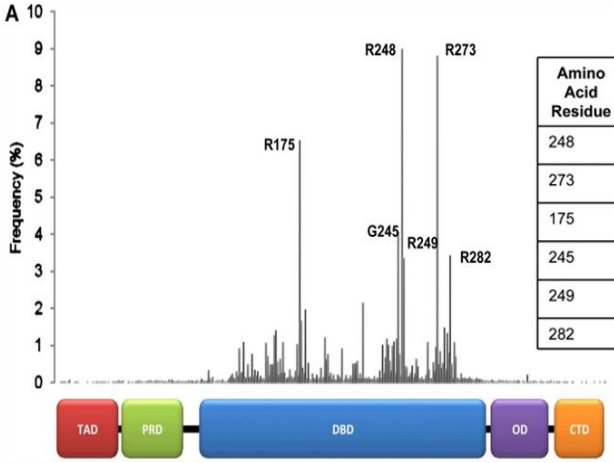

B

Amino Acid Residue	Frequency of Alteration
248	7.0%
273	6.7%
175	5.1%
245	3.3%
249	2.9%
282	2.9%

C

Mutation	Overall Frequency	Wild-Type Codon	Mutant Codon	CpG	Class
R175H	4.6%	CGC	CAC	Yes	Conformation
R248Q	3.5%	CGG	CAG/CAA	Yes	DNA Contact
R273H	3.1%	CGT	CAT	Yes	DNA Contact
R248W	2.8%	CGG	TGG	Yes	DNA Contact
G245S	2.8%	GGC	AGC	Yes	Conformation
R273C	2.7%	CGT	TGT	Yes	DNA Contact
R282W	2.4%	CGG	TGG	Yes	DNA Contact
R249S	1.8%	AGG	AGT	No	Conformation
G245D	0.68%	GGC	GAC	No	Conformation

Fig. 1.9: (a) Frequency of mutations in the DNA binding domain (b) Table for the frequency of mutation in the 6 'hot spot' residues (c) Table for the most common missense mutations with the frequency of occurrence and class of mutation[15].

The DNA-binding mutants i.e. R175H, R248Q and R273S used for the experiments constitute the most common hotspot p53 mutations in human cancer as shown in the figure above. R175H is a structural mutation that impairs the proper folding of the DNA binding domain while R248Q and R273S are contact mutations that do not perturb the structure but disrupt the DNA binding. These mutants are known to exhibit a dominant negative effect in a way that it can abrogate the wild type function by the formation of mutant-wild type heterotetramer[15]. Upon its aggregation, mutant p53 induces misfolding[14] and co-aggregation of wild-type p53 causing inefficient transcription of target genes that are important for cell growth control and apoptosis.

Hence, along with this and the gain of function property, it is no surprise that they are most frequently mutated in cancer. Evidence suggests that a cooperative model of DNA binding is employed with a Hill coefficient of 1.8[6] and mutations in the TD can decrease the overall binding affinity to the DNA, preventing the formation of stable nucleoprotein complexes. Since these mutations are not present in the TD, there is some uncertainty whether tetramer formation

would still persist in these mutants, or if DNA binding precedes tetramerization and is required for the nucleoplasmic accumulation of p53 tetramers.

Some of these questions are hoped to be answered by the N&B analysis and might shed some light on the sequence of events that takes place in vivo.

By obtaining the aggregation plots of wild type p53, a comparative study was established by conducting the same set of experiments and analysis with the mutant forms of p53.

CHAPTER 2

Background

p53 is one of the most extensively studied genes and proteins[28]. When it was first discovered in 1979, it was suspected to be an oncogene but a decade of research established that it was in fact a tumor suppressor which was mutated in cancer. Subsequent research followed and revealed its multifaceted functions as a transcription factor and in regulation of metabolism.

2.1 P53 as a tumor suppressor

P53 was suspected to be a tumor suppressor when the analysis of retrovirus insertion in an Abelson murine leukemia-transformed mouse cell line revealed the alterations in p53 specific genomic DNA sequences[29]. Similar observations were made by studying the leukemias induced in mice by Friend erythroleukemia virus. With further research, it became clear that p53 mutations are present in tumor derived murine cell lines and it was these mutants that were responsible for contributing to the tumor phenotype and not the wild type p53[30]. In vitro functional analysis showed that p53 alleles were frequently lost by mutations or deletions in colorectal tumor cells such that they did not retain any functional wild type[31]. In contrast to the transforming activities of tumor-derived p53 mutants, overexpression of wild type p53 repressed the transformation of cultured cells by activating oncogenes such as c-myc and H-Ras[32]. These data were evidence enough to confirm the tumor suppressive activity of p53. After this was established, further studies showed that p53 mutations were exhibited not only by colorectal

tumors but in fact half the tumor specimens examined. This makes it the most frequently mutated gene in human cancers[28].

2.2 p53 in regulating cell cycle

Cell cycle checkpoints are crucial following DNA damage and exist in most organisms. These cell cycle arrests, G1 & G2, ensure the prevention of both replication of damaged DNA and segregation of damaged chromosomes. During this transient delay, the damaged DNA is believed to be undergoing repair to resume its critical functions[33]. p53 was believed to participate in this mechanism by Kastan et al when an exposure of cells to IR demonstrated an increase in the p53 protein level that correlated with the termination of replicative DNA synthesis[34]. Following this, an exposure to IR failed to reproduce the same response of arresting G1 cycle in tumor cells expressing mutant p53. This observation was further extended by demonstrating that the loss of p53 alleles in murine fibroblasts resulted in a loss of G1 arrest following IR exposure[35]. With the use of a temperature sensitive mutant of p53, that exerts a wild type (wt) activity at 32°C but loses this activity at 37° C and higher, it was found that reconstitution of wt p53 could bring about a growth arrest not only at G1 but also at G2/M[36]. Therefore, this contributes to its tumor suppressive role by preventing the proliferation of abnormal cells.

2.3 p53 in apoptosis

Apoptosis, or programmed cell death, is a mechanism in which severely damaged irreparable cells are permanently removed from the proliferating cycle. The role of p53 in apoptosis was discovered when Oren and co-workers reported that the temperature sensitive mutant p53 induces apoptosis in myeloid leukemia cell lines at a temperature in which it is reactivated and

predominantly in the wild type conformation[37]. Since these cell lines are deficient in endogenous p53, the apoptotic ability of this protein was established. This was reconfirmed by the work carried out by Shaw and co-workers, in which the expression of wt p53 in colon tumor derived cell lines induced apoptosis in cells grown in vitro, prevented tumor formation in nude mice and brought about the regression of these tumors in vivo[38]. These findings established p53 as a mediator of apoptosis and provided evidence that apoptosis can serve as a mechanism of tumor suppression.

2.4 Number and molecular brightness analysis

It is a problem in cell biology to determine the number and brightness of molecules in living cells as the concentration and clustering of the protein differ in different locations within the cell and change in biological processes. This was made feasible by the use of fluorescence proteins and the earlier approaches involved evaluating the number of molecules in a pixel by calibrating the fluorescence intensity with a solution of known concentration. By this method, it was possible to achieve the number of fluorophores but difficult to decipher the oligomerization state since a small number of aggregated molecules may exhibit the same average intensity as many dim molecules[22]. This problem was partially resolved by Fluorescence correlation spectroscopy (FCS), where the number and brightness of the protein could be determined separately by a method of moment analysis[39]. This is sufficient for a homogenous solution of a single molecular species but for multiple species of different brightness, this method cannot be used. The photon-counting histogram (PCH) analysis was employed to overcome this limitation[40]. PCH is capable of determining the number and brightness of multiple species but requires a large number of observations per pixel and hence is computationally too slow to map the aggregation of protein

across an entire cell. The Number & molecular Brightness (N&B) approach is used to map the oligomerization state in cells within seconds by pixel moment analysis. The number (N) and brightness (B) of proteins is measured by the first and second moment of fluorescent intensity distribution at each pixel. It takes into account the immobile fraction, slow moving features and bleaching which are usual in cell measurements.

N&B analysis was used to demonstrate the number and brightness of the EGFP molecule in CHOK-1 cells[22]. The monomeric GFP accumulates primarily in the cytosol with the homogeneous brightness and heterogenous population of molecules as shown below in Fig. 2.1. Since the GFP exists in the monomeric form with the absence of higher order aggregates, the map of molecular brightness is uniform. The number of GFP molecules is different at different regions and shows a lower distribution at the cell borders.

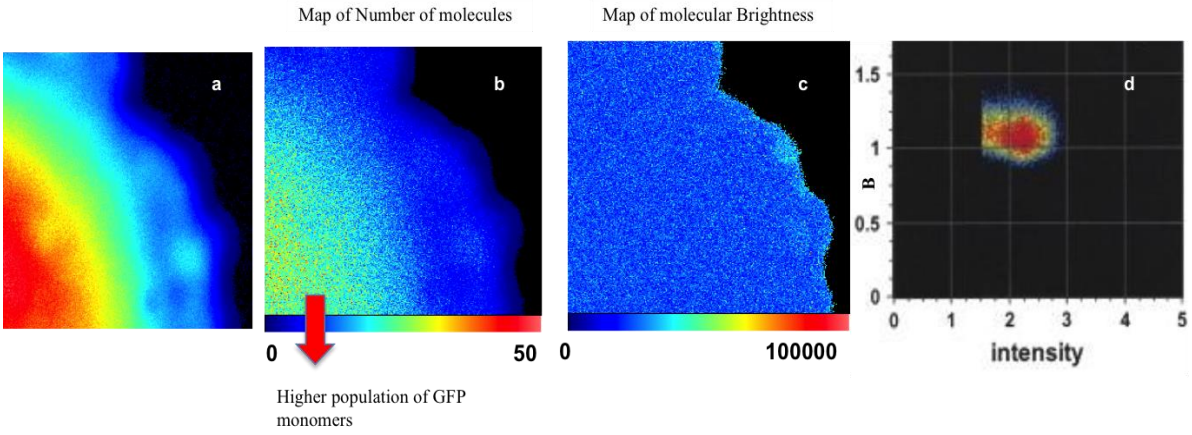

Fig. 2.1: N&B analysis on CHOK-1 cells [22] (a) Average intensity of CHOK-1 cells transfected with EGFP (b) A higher population of GFP exists near the cytosol as shown by a higher intensity at that region (c) EGFP molecules exhibit the same brightness due to their monomeric state hence uniform distribution is seen. (d) Map of apparent brightness vs. intensity reveals the monomeric brightness between 1 and 1.5.

The N&B method was also employed to detect and quantify molecular aggregates by studying the binding and unbinding of paxillin-GFP to adhesions in CHO-K1 cells. Paxillin is shown to be primarily monomeric in the cytosol and exists as higher order aggregates at regions of adhesions during the unbinding process [22]. The process of binding and unbinding is represented at a high spatial resolution as shown below.

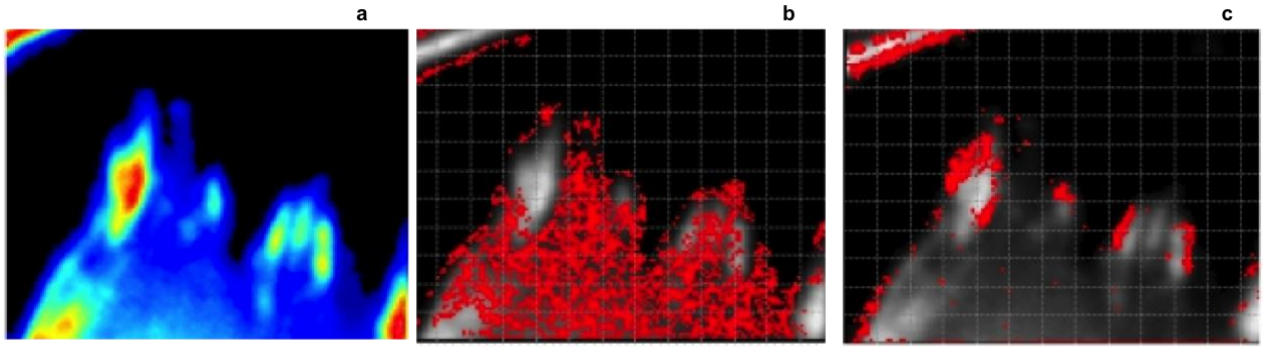

Fig. 2.2: Paxillin EGFP in CHO-K1 cells (a) Average intensity of CHO-K1 cells show Paxillin accumulating at the focal adhesions (b) GFP monomers are selected in the histogram of B vs. intensity and is shown to accumulate in the cytosol denoted by the red pixels (c) Higher order aggregates are selected that correspond to paxillin aggregates at the region of the adhesions

CHAPTER 3

Materials & Methods

3.1 Primary cell culture

NIH3T3 fibroblasts grown in our lab were used in all the experiments as it is one of the most widely studied cell lines, is transfected with ease and does not exhibit any traits of a cancerous phenotype. These cells were grown with Dulbecco's modified Eagle's medium (DMEM) supplemented with 10% fetal calf serum (FCS), penicillin G (100 units/ml), and streptomycin (100 ug/ml) and maintained at 37ºC in a humidified 5% CO_2 incubator. Prior to the experiments, the cells were trypsinized and plated on 6ug/ml fibronectin coated 8-chambered Lab Tek® imaging dishes. For the cells with anisomycin treatment, 35mmx10mm Corning imaging dishes were used. They were allowed to attach 24 hours before transfection with lipofectamine 2000 (invitrogen) and the p53-EGFP plasmid that was purchased from Addgene. The same protocol was followed for transfection with the mutant p53-EGFP plasmids. Cells were also transfected with plasmid coding only GFP to establish and normalize the brightness of GFP monomer.

3.2 Plasmids

EGFP and the p53-EGFP (Plasmid #11770) plasmids were purchased from Addgene (www.addgene.org). These plasmids were maintained by further amplification in transformed DH5 alpha strain of E.Coli cells. The p53 mutant-EGFP plasmids (L344A-GFP, L344P-GFP,

R273S-GFP, R248Q-GFP, R175H-GFP) were constructed and provided by Drs. Jane and Lee Bardwell (Bardwell Lab at University of California, Irvine).

3.3 Microscope setup

The Zeiss LSM 710 is a confocal microscope used for data acquisition. It consists of an incubation system where the cells are kept at 37ºC and 5% CO_2 24 hours post transfection. The EGFP was excited at a wavelength of 488 nm using an argon ion laser set to 1% laser power. A stack of 100 raster-scanned frames was acquired at a pixel dwell time of 6.3us/pixel with a frame size of 256x256. When imaging was done in less than three wells at a time, the same cells were tracked using the automatic stage positioning option between scanning. Each cell position was saved with spatial coordinates for sequential imaging between cells at a given time interval of 30min or longer. The stressing agents i.e. anisomycin, cisplatin etc. are added to the dishes and imaged for a period of 30 minutes to 4 hours depending on the type of experiment.

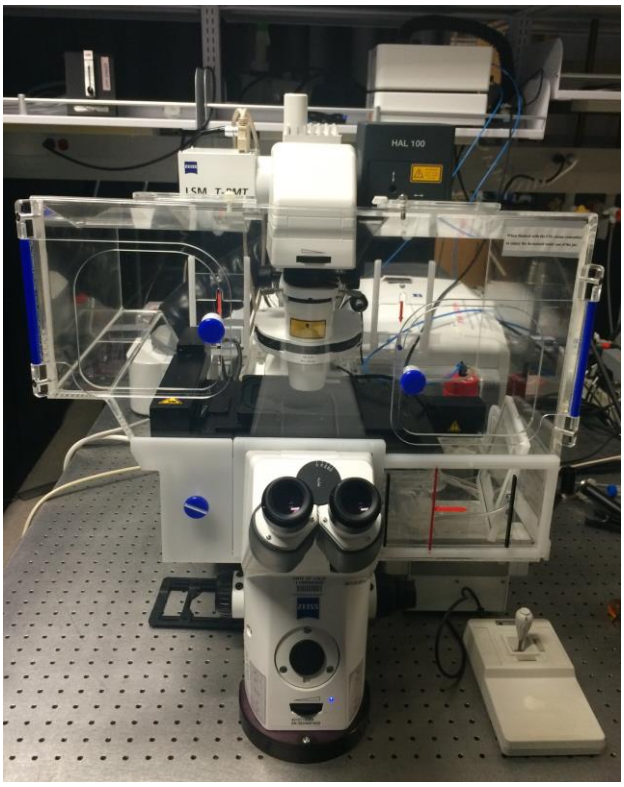

Fig 3.1: Zeiss LSM 710 confocal microscope

3.4 Experimental procedure

3.4.1 Experiments with cisplatin

The cisplatin powder was purchased from Sigma Aldrich. A low dose of the drug, 20µM, is administered to the cells and since this treatment takes longer to produce a noticeable change, cells were imaged for a period of four hours. Prior to the experiments, a fresh batch of 1mM cisplatin soln. dissolved in 0.9% NaCl was prepared every time. This was done by dissolving 3mg of cisplatin powder in 10 ml 0.9% NaCl and mixed till the powder dissolves completely. 0.9% NaCl was used since cisplatin has a tendency to decompose in aqueous solutions due to reversible substitution of water for chloride ions. The stability is enhanced in sodium chloride solutions due to the excess of chloride ions available[41]. The cells transfected with only GFP were

left overnight to allow sufficient transfection and then imaged to establish the monomer brightness. Following this, the cells transfected with p53-GFP is placed on the incubator of the microscope since the experiment was carried out for four hours. Cells are picked by eye through the brightfield/epi fluorescence microscopy pathway and only very dim cells were selected in order to somewhat replicate the endogenous concentration of p53. There were many overexpressed cells and care was taken not to select those. Once a handful of cells were located, their positions were saved with the purpose of following the same cell for the period of four hours. 20µM of the freshly prepared cisplatin solution was added to these cells and recorded as time 0. The soln. is added to GFP as well. A stack of 100 raster-scanned frames was then acquired at time 0, 60, 120, 180 and 240 minutes. Over the course of the experiment, it is not always feasible to follow the same cell and in that case, cells were selected every hour. At the end of the experiment, the cells started to look very unhealthy with a lot of dead, floating cells and debris.

The experiment is carried out in a similar fashion with NIH3T3 cells expressing mutant p53. These cells are plated on an 8 well imaging dish so that the experiments with all the different types of mutant p53 can be carried out simultaneously. The cells in each well are transfected with different plasmids namely GFP, L344A-GFP, L344P-GFP, R273S-GFP, R175H-GFP, R248Q-GFP and the p53-GFP that is used as a positive control. Once suitable cells were selected, 20µM of the cisplatin solution was added to each well and recorded at time 0. Images were then acquired at time 0, 60, 120 and 240 minutes for cells in each well.

3.4.2 Experiments with Anisomycin

A 10mg/ml anisomycin solution in DMSO was purchased from Sigma-Aldrich. A 1mg/ml stock solution was prepared and stored in -80°C. Individual dishes plated with NIH3T3 cells are prepared for each plasmid in this case as the experiments last for a 30 minute period and therefore back to back data acquisition can be carried out. A total of 7 dishes are transfected with the plasmids encoding GFP, p53-GFP, L344A-GFP, L344P-GFP, R273S-GFP, R175H-GFP and R248Q-GFP separately and left overnight. The experiment is carried out by selection of cells followed by addition of 500nM anisomycin solution. The same cells were followed in this case and images were acquired for a period of 30 minutes post anisomycin treatment at time 0, 10, 20 and 30. This is repeated for each dish.

These experiments were carried out multiple times in order to obtain a trend in the cells and reconfirm the data.

3.4.3 Experiment with NaCl

NIH3T3 cells expressing p53-GFP were used for this experiment. After cell selection, 130mM NaCl was added to the cells in addition to the salt already present in the culture media to maintain a hyperosmotic environment of 240mM NaCl. The time scale of p53 activation was unsure in this case and was repeated for different observation time with images acquired for a period ranging between 10 minutes to 4 hours.

3.5 Data Analysis

The acquired N&B data was processed by the SIMFCS software developed by the Laboratory for Fluorescence Dynamics at University of California, Irvine. Calibration of the monomeric brightness was performed by measuring the brightness of EGFP under the same experimental conditions. EGFP has an apparent brightness of 1.2 and an apparent brightness of dimers and tetramers correspond to 1.4 and 1.8 respectively by the relationship given by the equation below,

$$B = \varepsilon n + 1 \quad (9)$$

where B is the apparent brightness, n is the number of units corresponding to the oligomer state, e is the individual molecular brightness and 1 is due to the background/ immobile fraction.

CHAPTER 4

Results & Discussion

Cells with a medium level of expression were selected for imaging as shown below. Consistency in the selection process is crucial as overexpression of the protein can alter the results as explained in this discussion.

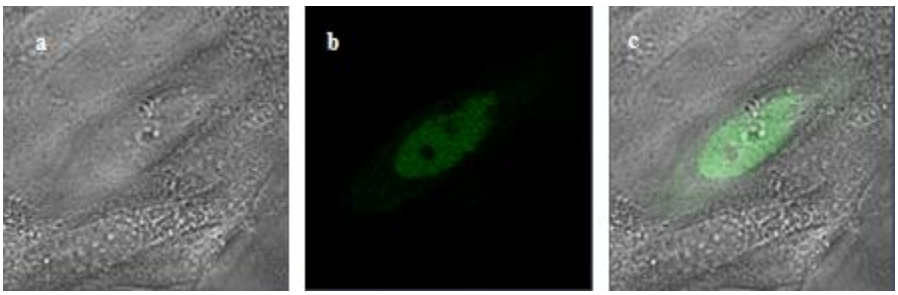

Fig. 4.1: (a) Brightfield image of a single NIH3T3 cell (b) Image of the same transfected cell acquired in the green channel (c) Combination of the two channels

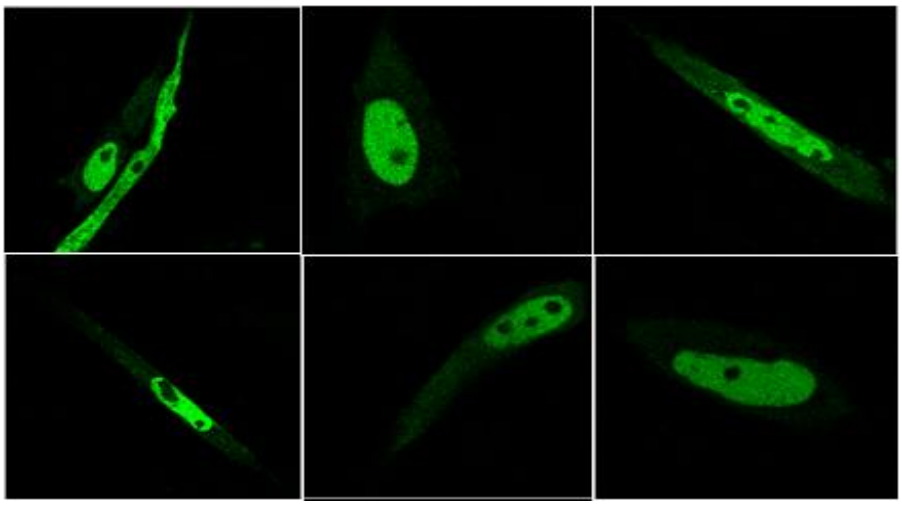

Fig. 4.2: Images of NIH3T3 cells transfected with p53-GFP excited at 488 nm

4.1 Number and Brightness analysis

The N&B analysis of NIH3T3 cells transfected with GFP alone reveal the presence of mainly monomers represented by the dark green colour as seen below. Very few dimers (lime green pixels) and absence of higher order aggregates (red pixels) are observed. The apparent brightness of monomers and dimers are at approximately 1.2 and 1.4 respectively as seen in the intensity vs. brightness map.

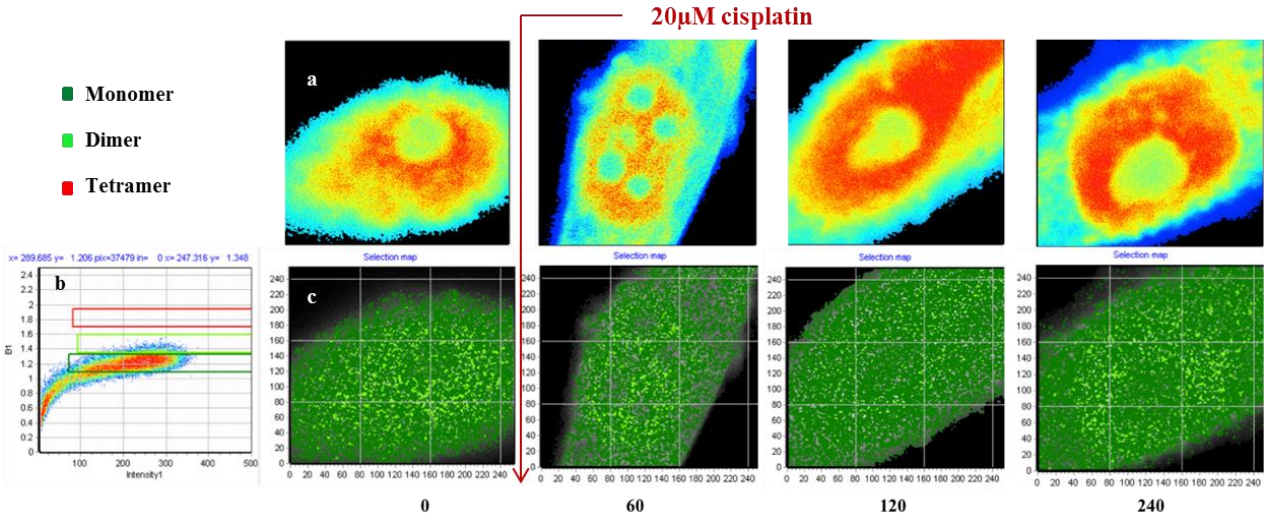

Fig. 4.3: N&B analysis of NIH3T3 cells (a) Average intensity of cells transfected with GFP (b) 2-dimensional plot of apparent brightness vs intensity reveals the monomeric and dimeric brightness at 1.2 and 1.4 respectively (c) GFP monomers and dimers are selected in the histogram and are uniform throughout the time period ranging from 0-240 minutes

In contrast, The N&B analysis of NIH3T3 cells transfected with p53-GFP reveals the presence of higher order aggregates post DNA damage. Tracking of the same cell over time was done to better assess the sequence of events. As seen from the figure below, there are three distinct populations. The monomer distribution is restricted to the cytoplasm while there is a higher accumulation of dimers throughout primarily in the nucleus. A third population of aggregates

corresponding to a brightness of 1.8 is observed after DNA damage, shown by the red pixels. The accumulation of these aggregates increases with respect to time.

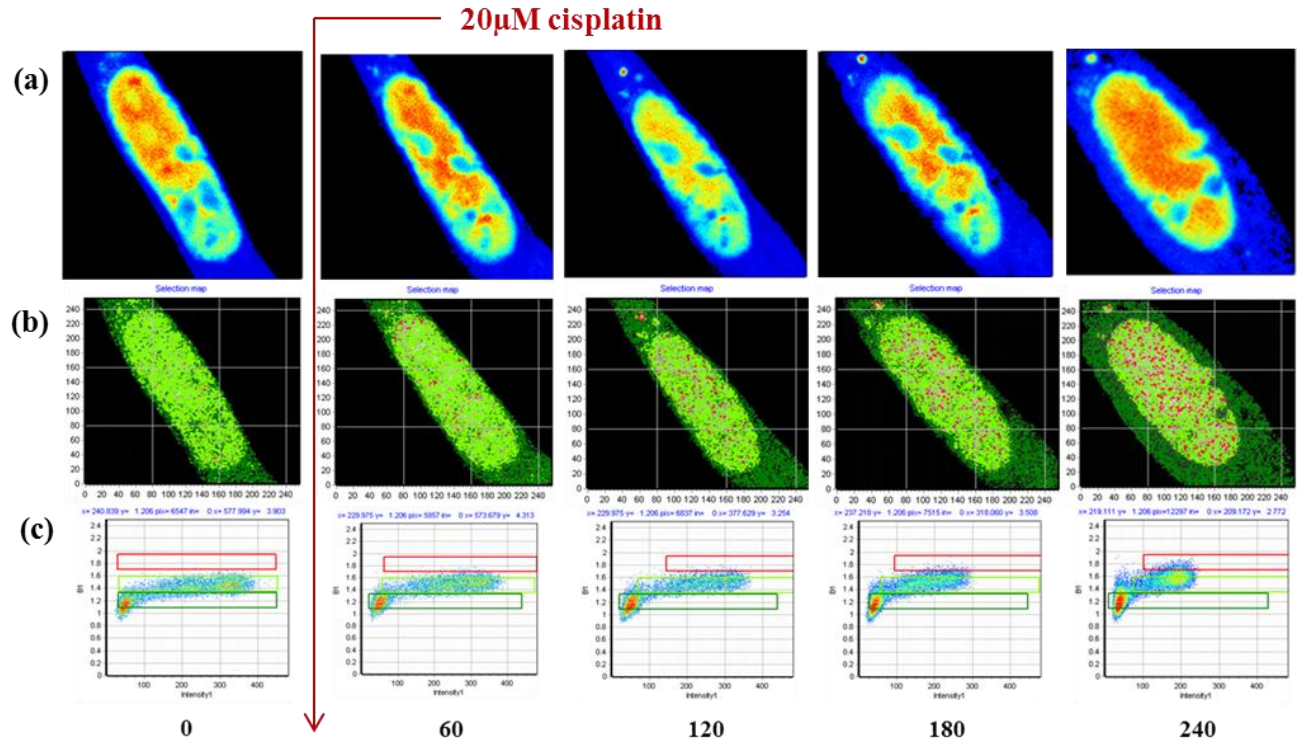

Fig. 4.4: Single cell N&B analysis as a function of time with DNA damage (a) Average intensity maps of NIH3T3 cells transfected with p53-GFP at 60 minute intervals after treatment (b) Distribution of the aggregation states of the p53-GFP selected from the corresponding brightness values in the histogram. An increase in the accumulation of red pixels is seen at every time point and reaches a maximum level at 240 minutes (c) Intensity-brightness histogram in which the distribution is linear at time 0 and increases gradually over time

The population of the 3 distinct aggregation states observed above is represented as a function of time.

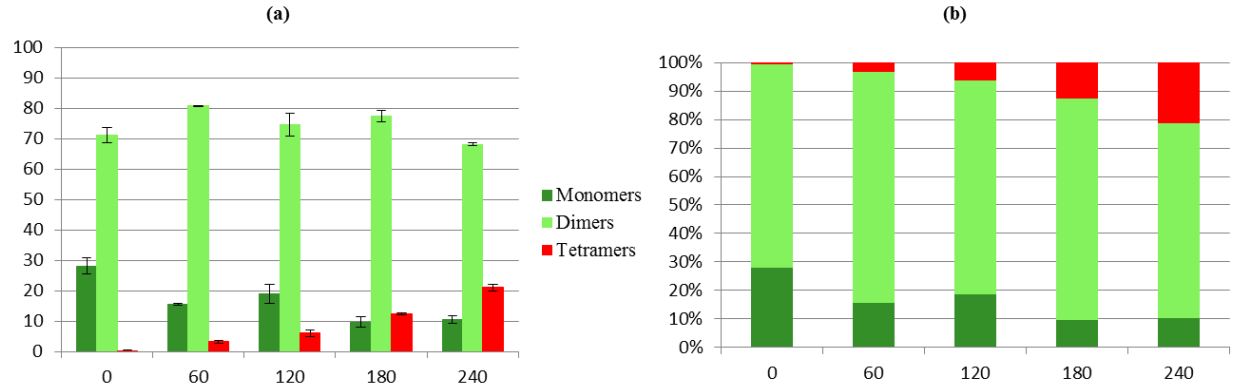

Fig. 4.5: (a) Representation of the different aggregation states of p53-GFP plotted with respect to time (b) % of aggregate population at a given time

NIH3T3 cells transfected with p53-GFP were next treated with anisomycin and the N&B analysis of these cells is shown below. In contrast to the cisplatin, stimulation with anisomycin led to a dramatic increase in the presence of higher order aggregates within 10 minutes as depicted in the B versus intensity histogram. A profound increase in the concentration of tetrameric p53-GFP at 30 minutes was established.

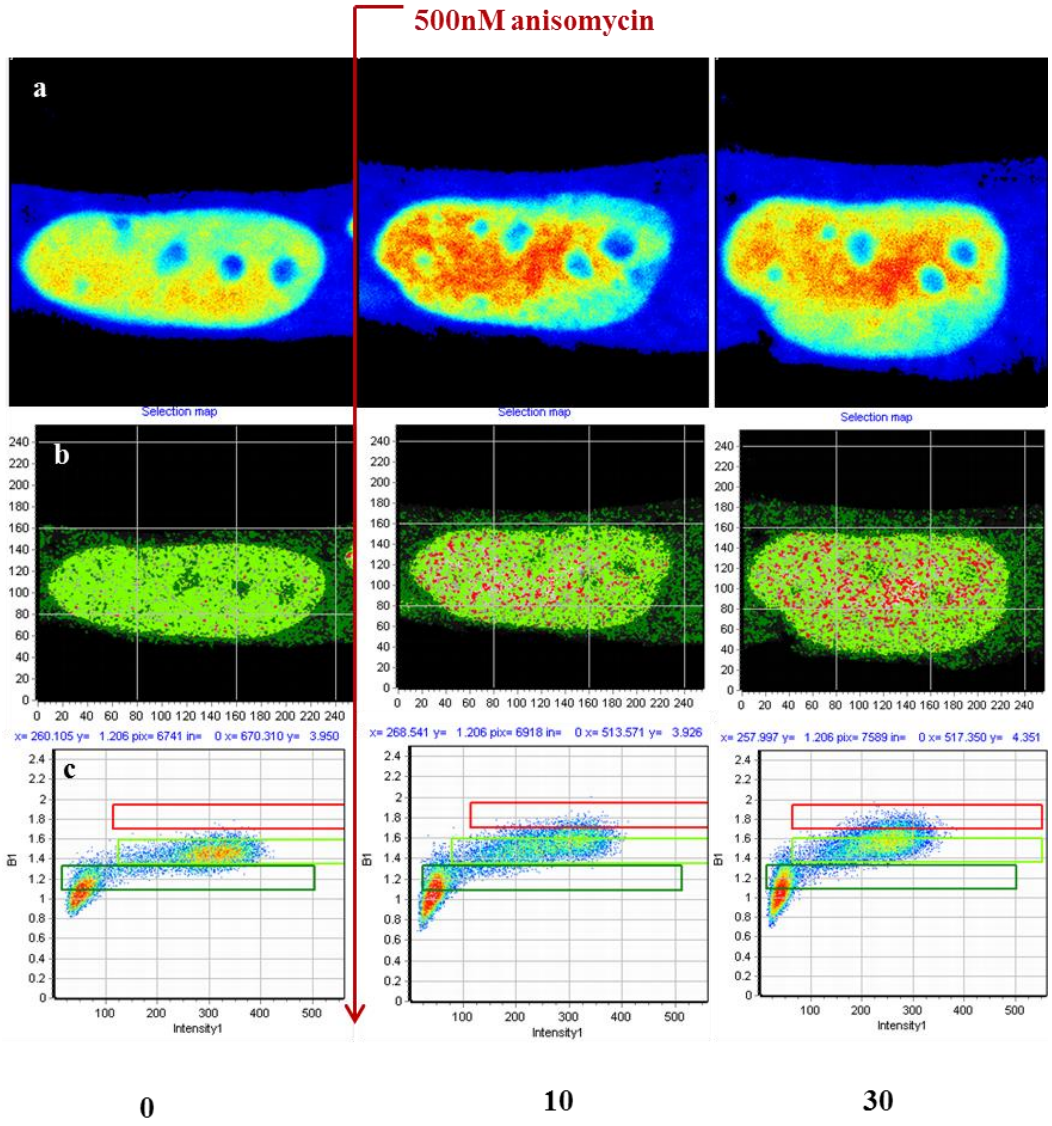

Fig. 4.6: Single cell N&B analysis as a function of time with ribotoxic stress (a) Intensity map of NIH3T3 cells expressing p53-GFP before and after treatment of anisomycin (b) Derived brightness map reveals the increase in tetramer level with time (c) Intensity versus brightness plots show a higher population of pixels corresponding to a brightness of 1.8 after addition of anisomycin

The monomer, dimer and tetramer population of p53-GFP in cells exposed to DNA damage and to ribotoxic stress were plotted as a function of time and compared to observe the trend between them.

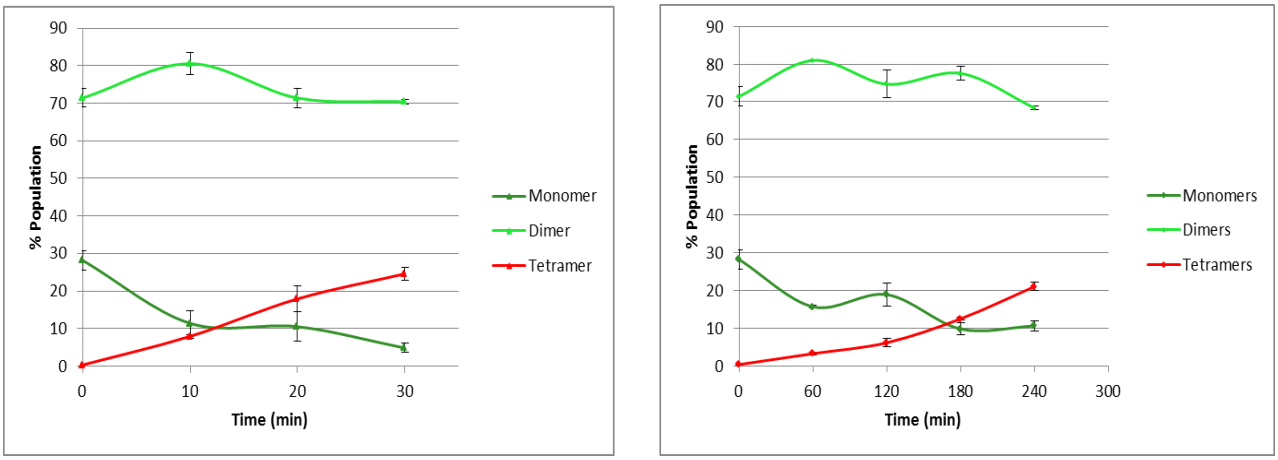

Fig. 4.7: Comparison of population of p53-GFP oligomers between cells stimulated with (a) Ribotoxic stress in the form of anisomycin and (b) DNA damage brought about by cisplatin. N=7 cells were imaged at each time point and standard deviation calculated from the mean of data at those points.

The same experiments were carried out for each mutant form of p53-GFP and analyzed. The same cells could not be followed in this case. One mutant form of p53-GFP exhibiting mutation in the tetramerization domain and one in the DNA binding domain are represented below. Images of all the mutants are not included due to redundancy but population of all the mutant aggregates are depicted in fig. 4.9.

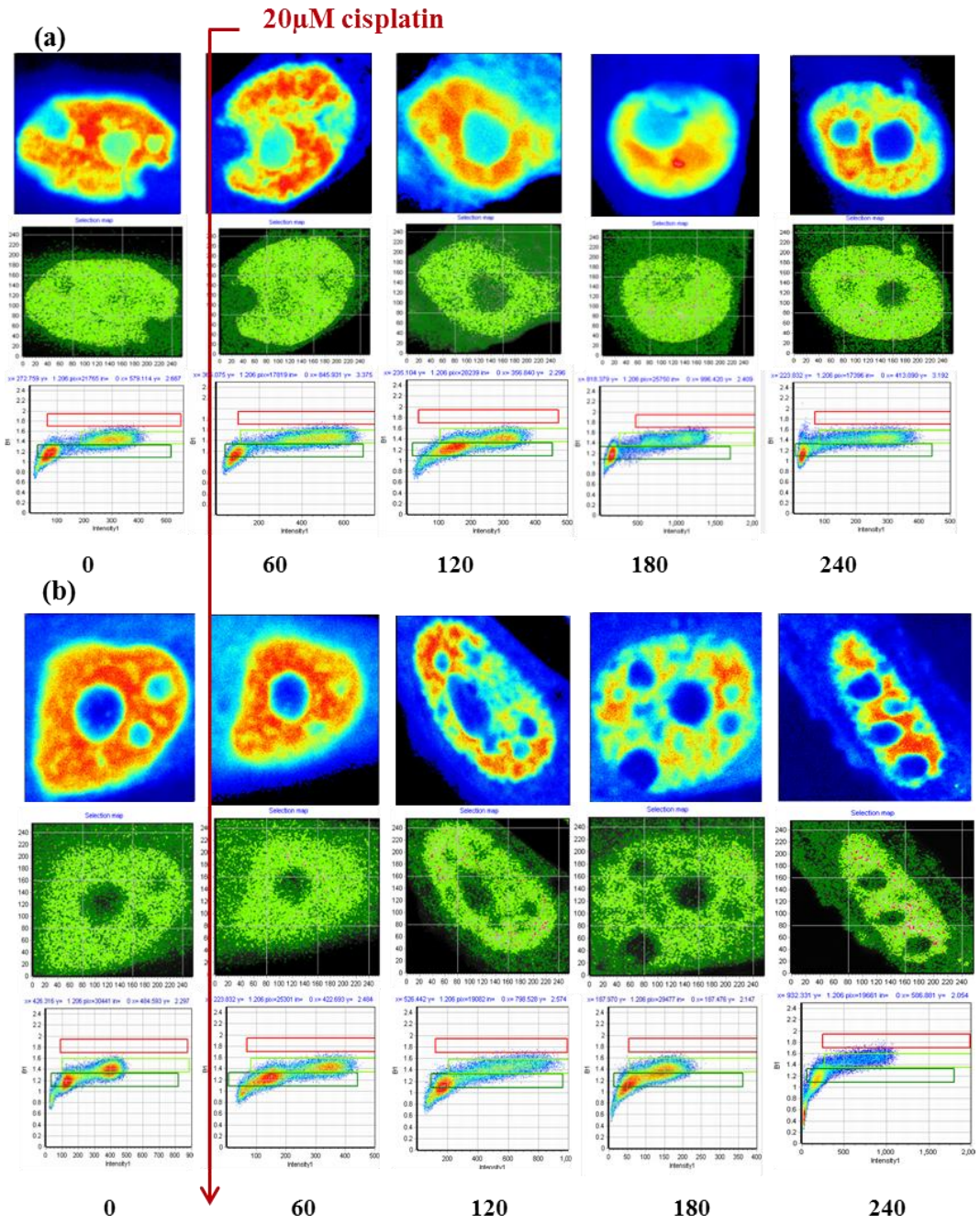

Fig. 4.8: N&B analysis of NIH3T3 cells expressing mutant forms of p53-GFP with DNA damage (a) Intensity and brightness maps of L344P-GFP, mutant form of p53-GFP in the tetramerization domain (b) Intensity and brightness maps of R175H-GFP, structural mutant in the DNA binding domain

The populations of tetramers observed in each mutant form of p53-GFP after induction of stress are plotted below:

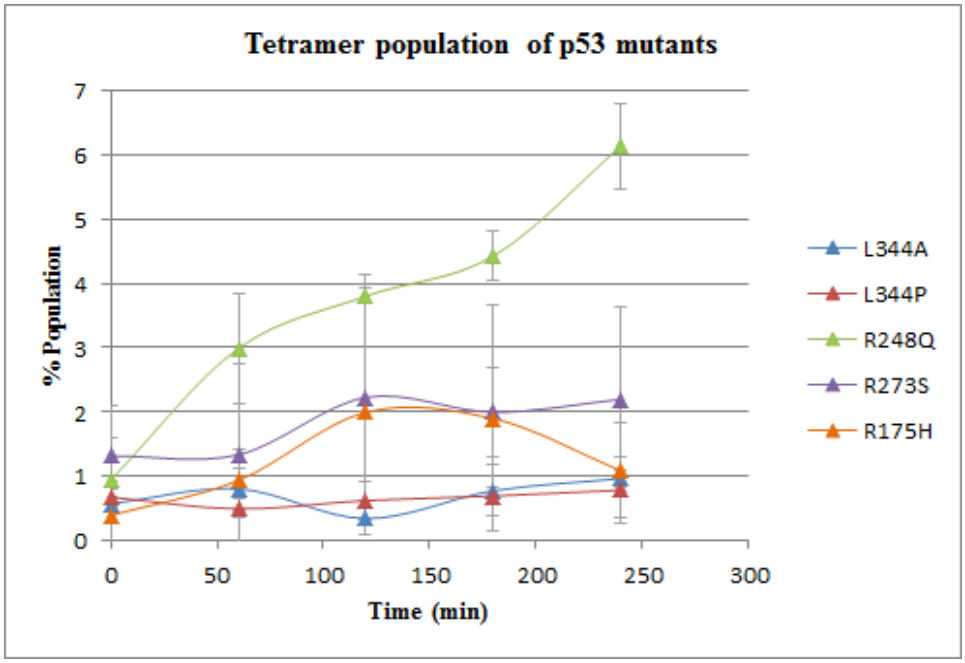

Fig. 4.9: % Population of the p53 mutant tetramers with DNA damage

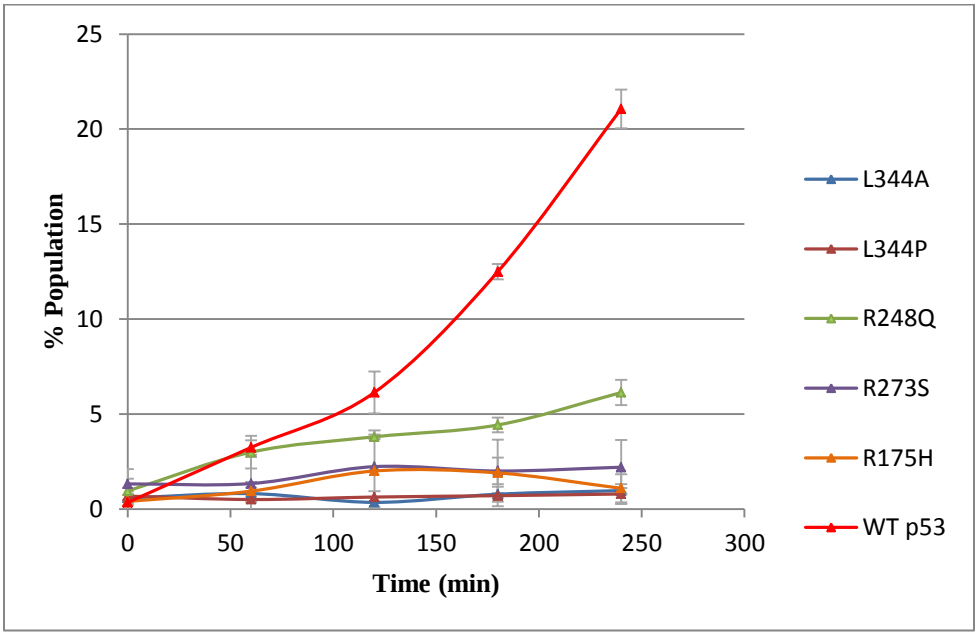

Fig. 4.10: Comparison of tetramer population of p53 mutants with the wild type after DNA damage

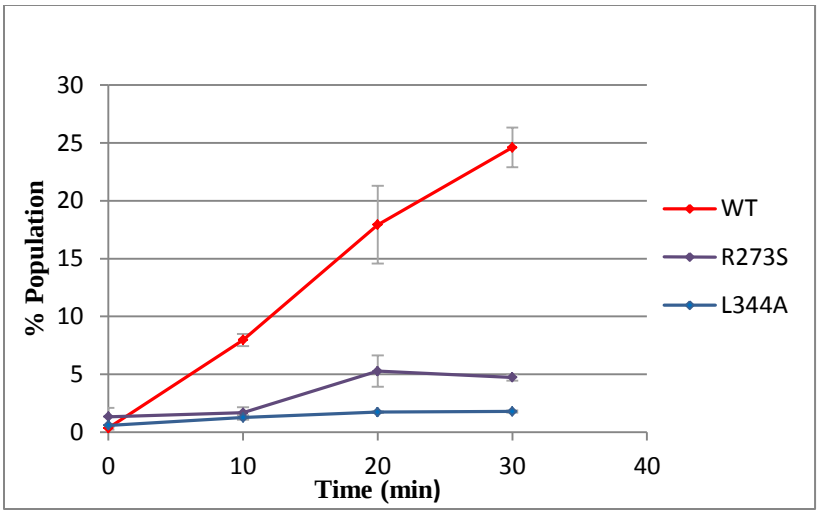

Fig. 4.11: Comparison of the tetramer population of a DNA binding mutant, TD mutant and wild type p53-GFP after ribotoxic stress

Experiments with the addition of 130mM sodium chloride solution on NIH3T3 cells expressing p53-GFP were carried out to observe the effect of osmotic stress on the p53 protein. Similar to anisomycin exposure, the response is quick and substantial within 20 minutes post treatment.

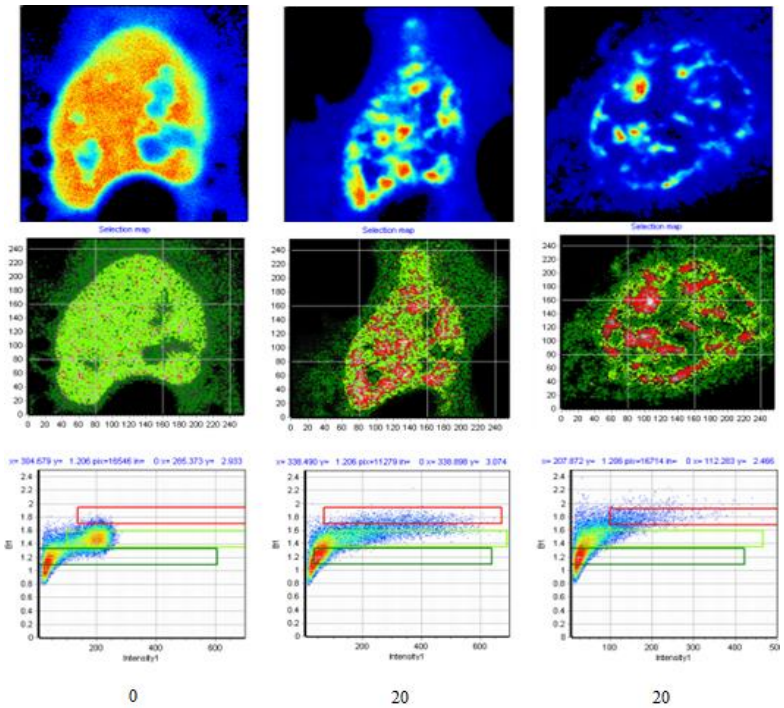

Fig. 4.12: N&B analysis of NIH3T3 cells expressing p53-GFP on exposure to environmental stress. (a) Intensity map, brightness map and Intensity vs. brightness histogram of cell before stress (b) Increase in tetramer levels of the same cell after 20 minutes (c) Increase in tetramer levels of a different cell after 20 minutes

Testing of the reactivation of R175H-GFP to restore wild type function and induce tetramerization was carried out post DNA damage by addition of a therapeutic compound under investigation. The images below represent the R175H-GFP with and without reactivation after a period of 4 hours to observe the presence of higher order aggregates.

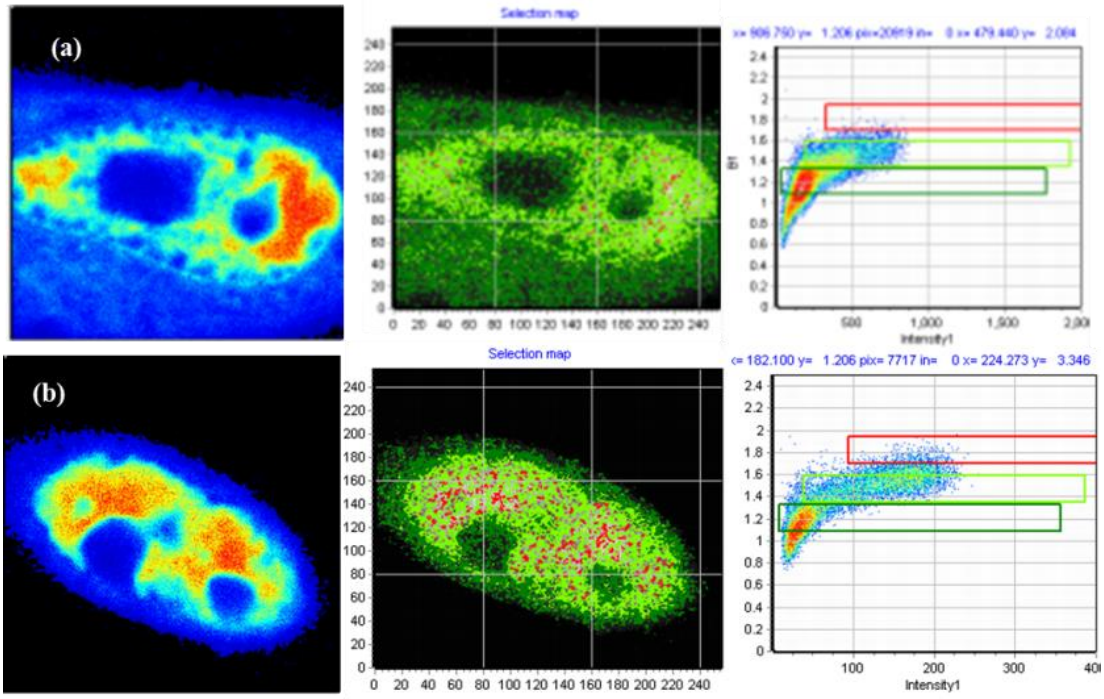

Fig. 4.13: N&B analysis of NIH3T3 cells expressing R175H-GFP after a period of 4 hours following cisplatin treatment (a) Without the compound (b) With the compound

4.2 Discussion

As seen in the results, it is evident that there is a gradual increase in the accumulation of p53-GFP aggregates, specifically tetramers as a function of time in cells expressing p53-GFP on addition of stressing agents namely cisplatin, anisomycin and sodium chloride soln. The aggregation is observed essentially in the nucleus with the cytoplasm consisting of mostly p53 monomers. In contrast, the N&B analysis of cells expressing GFP alone is dominated by a high population of monomers, as seen in fig. 4.3, and is consistent ranging from 95.83±0.22% to 94.2±0.95% at time 0 and 4 hours respectively. The dimer population is relatively low throughout starting from an initial population of 4.3±0.23% and increasing very slightly to 5.8±0.96% at the end of 4 hours. There is absolutely no tetramer population observed in these cells hence serving as a good control. It is interesting to see the behavior of p53 in response to cellular stress in vivo, thereby confirming the necessity of oligomerization in order to carry out its specific functions.

In case of DNA damage, the tetramers start accumulating within one hour of cisplatin damage and reach its peak at 4 hours as seen in fig. 4.4. The images are acquired at hourly intervals as the action of cisplatin is relatively slower. After this time period, some of the cells start rounding up and begin to undergo apoptosis. In fig. 4.5, the population of the different p53-GFP aggregate states i.e. monomers, dimers and tetramers are plotted as a function of time. The cells are masked to isolate the region of interest i.e. the nucleus, as there are no higher order aggregates in the cytoplasm. There is a gradual decrease of monomer population compensated by an increase in tetramer population, reaching its peak of about a 21.05±1.02% population at 4 hours. The p53-GFP also exhibits a consistent high dimer concentration (70-80%) throughout which may be the

driving mechanism for tetramer formation as a dimer-dimer aggregate. The tetramers that are formed show evidence of the fact that they are required to bind to the DNA and regulate its transcriptional function. In comparison, the data with the mutants show a significantly reduced population of tetramers that is consistent with our expectations. The N&B analysis of the TD mutants (L344A and L344P) reveal an insignificant increase in the population of tetramers from time 0 to 240 as represented by the L344P-GFP mutant in fig. 4.8(a). The DNA binding mutants compared to the TD mutants exhibit a higher tetramer accumulation with respect to time but are relatively at a much lower percentage to the tetramer population seen in the wild type and this can be elucidated in fig. 4.9 and 4.10. The N&B analysis of the DNA binding mutant R175H-GFP is shown in fig. 4.8(b). Out of the 3 DNA binding mutants, R248Q seems to exhibit a higher increase in the percentage of tetramers, having a maximum value of 6.13±0.67% at 4 hrs. R273S and R175H have a maximum tetramer population of 2.2±1.4% and 1.09±0.74%. Contact mutations, R248Q and R273S have very little effect on the ability of the p53 protein to fold and therefore are very similar structurally to wild-type p53. On the other hand, structural mutations, such as the R175H have a significant effect on protein folding causing destabilization of the protein structure[42]. This may explain why there is a lower population of tetramers of the R175H mutant as compared to the other two DNA binding mutants. Nevertheless, since these mutations are in the DNA binding domain, there seems to be no reason why tetramerization would be completely inhibited and an intermediate level of residual tetramers seems consistent with my expectation. In addition, it has been previously observed that the activity of mutant p53 also depends on the level of expression[19]. Due to their high Kd value of tetramer formation, higher levels of these mutant proteins may be required for efficient tetramerization and can be achieved by overexpression. Since the levels of p53 used for these experiments are 3-5 times the

endogenous levels, this is a possibility. This can also explain why a tetramer population, although trivial, exists for L344A and L344P. However, I believe that these tetramers, owing to its small population may not be sufficient to induce a stress response. Moreover, they may form unstable complexes that bind transiently with the DNA but are unable to form a stable nucleoprotein complex required to regulate normal transcriptional activity[6]. A comparison of the mutant tetramer population with the wild type after DNA damage is shown in fig. 4.10.

The experiments with anisomycin shows similar results as seen in fig. 4.6 but since anisomycin acts much faster, the time scale of observation is smaller. The accumulation of p53-GFP tetramers is pretty evident at 10 minutes into the experiment and by 30 minutes there is a substantial increase in this accumulation. Due to the very high population of tetramers, it is hard to decipher the exact localization of binding sites but we suspect aggregation to be predominant especially at regions around the nucleolus. Fig. 4.7(a) shows the population of p53 aggregates on addition of anisomycin. It is interesting to note that it follows the same trend as the cisplatin data (4.7b). The high dimer population remains fairly consistent throughout (70-80%) while there is a gradual decrease and increase in the monomer and tetramer population respectively. The percentage of tetramers increases by 24.27±1.84% from its starting value while the monomer population decreases by 23.37±2.39%.

The experiment with sodium chloride soln. was carried out to introduce environmental stress and assess the difference in p53 response mechanisms depending on the type of stress. The response is almost immediate after addition of NaCl soln. with a drastic accumulation of p53-GFP tetramers within 20 minutes as seen in fig. 4.12, and is followed quickly by cell death. The populations of monomers, dimers and tetramers after 20 minutes are 12.9±4.7%; 59.16±6.8% and 27.8±2.6% respectively. In this case, it is striking to witness the nuclear fragmentation of

cells so promptly and this being a hallmark of apoptosis, validates the need of tetramerization for efficient p53 regulation.

As discussed in the introduction, p53 has a dual role in mediating either repair mechanisms or cell death depending on the level of stress. From the data above, it is clear that at a higher level of damage, p53 induces genes to regulate apoptosis especially in the case of environmental stress. Since cisplatin acts slowly and the amount added to the cells isn't sufficient to induce a dramatic response immediately, the cells look fairly fine during the span of observation. These cells may be undergoing a DNA repair mechanism to prevent the proliferation of damaged cells. However, there are certain cases in which the nucleus starts rounding up followed by a nuclear fragmentation and/or blebbing after 4 hours, especially in cells expressing p53-GFP at higher levels which leads me to believe that in the presence of stress, the intracellular level of p53 regulates the switch between repair and apoptosis.

One of the problems encountered in a few cases was the accumulation of tetramers even before the induction of stress, which could explain tetramerization as a concentration dependent process. A high local concentration of p53 could force self-assembly into tetramers in the absence of stress signals. As discussed previously, since the levels of p53-GFP used for these experiments are much higher, it is a possibility that overexpression contributes to this effect.

There was some uncertainty regarding the interference and participation of endogenous p53 in the complex formation. However, since the endogenous levels of p53 in unstressed NIH3T3 cells is comparatively low and the rate of increase of p53 concentration in response to stress is relatively slow, interference in the formation of heterodimers with the human p53-GFP was not to be encountered. For additional measures and further clarifications, experiments were repeated in p53 knockout cells and yielded similar results (data not shown).

The reactivation of the mutant R175H-GFP was carried out with the addition of a potential therapeutic candidate and observed for the presence of higher order aggregates namely tetramers. R175H being a structural mutation, impairs the proper folding of the protein bringing about a destabilization of the structure. By targeting to stabilize the protein, p53 activity can be restored[43]. The same protocol of DNA damage in R175H-GFP transfected cells was followed as mentioned in the material & method section prior to the addition of this compound. Data acquisition and analysis were carried out in a similar fashion. With N&B analysis, the presence of a higher population of tetramers was observed in these cells at a 4 hour time point compared to the data without reactivation as shown in fig. 4.13. On observation after a longer time period, most of the cells are dead and detached. Based on these results, the tetramerization of p53-GFP is stimulated and the restoration of the wild type activity seems to be successful. However, this is preliminary in vivo testing and further investigation, especially in cancer cells, will be carried out to check the viability of these results.

4.3 Conclusion and Future Directions

From my research, the crucial role and necessity of p53 tetramers in maintaining homeostasis has been established in vivo and a further expansion of this study in cancer cells and animal models would reaffirm these findings. So far, it is evident that p53 loses its tumor suppressor activity when mutated, contributing to the malignant phenotype. This characteristic makes it an attractive target for drug development. The study of murine models of cancer indicates that restoring the function of wild-type p53 in tumors is highly therapeutic and in some instances curative[44]. Hence, extensive research over the past few years has made it possible to develop such novel anti-cancer therapies that strive to either activate p53 or reactivate its function in tumors by

changing the conformation of mutant p53. A demonstration of that effect was provided in the section above. Numerous drugs and compounds have already been identified in the recent years and many more are in the stages of being approved by the FDA[45]. With the results of my research being favourable so far, I have no doubt that in the near future; targeting this fundamentally critical protein could provide a breakthrough in the field of cancer treatment thereby revolutionizing the current cancer therapies.

CHAPTER 5

p53 and Metabolism

5.1 Introduction

It is well established that cancer cells acquire a number of alterations to maintain their malignant phenotype. They are characterized by rapid proliferation, resistance to apoptosis and an altered interaction with the microenvironment. This rapid proliferation of tumors requires a large quantity of energy that drives metabolic reprogramming of these cells using alternate pathways for energy production. The metabolic transformation allows cancer cells to grow and divide unchecked with the ability to flourish in a hostile environment. As we all know, this transformation is in the form of the Warburg effect[2]. The Warburg effect is exhibited by essentially all cancer cells and is characterized by a high rate of glycolysis under aerobic conditions. Glycolysis involves the breakdown of glucose to pyruvate in the cytosol and is an alternative energy-producing pathway to oxidative phosphorylation. Normal cells under normal conditions exhibit Oxidative Phosphorylation (OxPhos), a mitochondrial process where ADP is phosphorylated to ATP as a direct consequence of oxidizing NADH to FADH2. OxPhos is the most efficient way of energy production and compared to glycolysis, it produces larger amounts of ATP per molecule of glucose[46]. Nevertheless, glycolysis is a much faster process and this is preferred due to the high rate of proliferation seen in cancer cells.

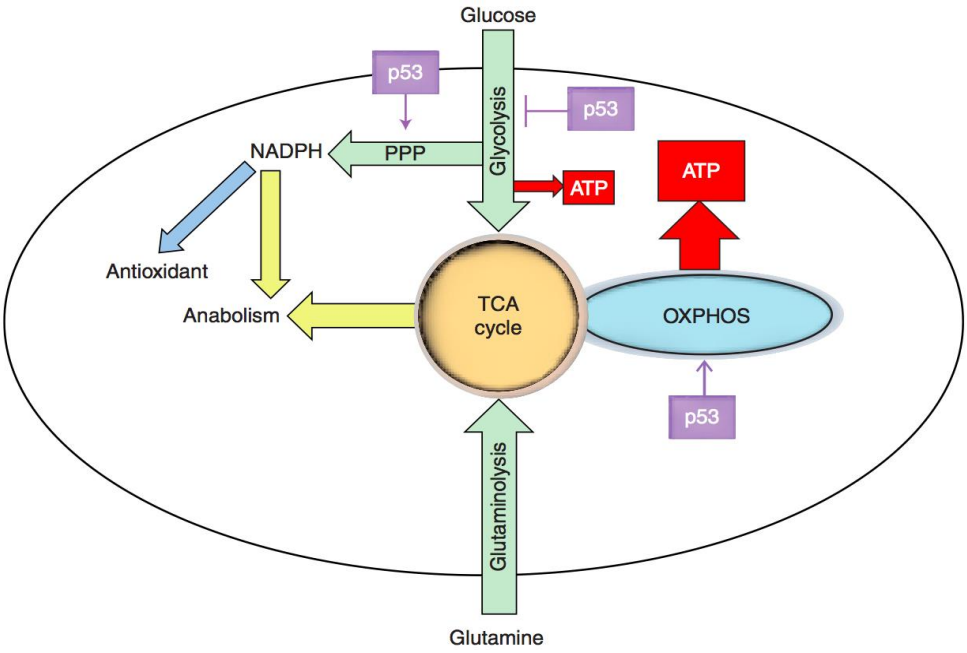

Fig. 5.1: p53 regulation of energy producing metabolic pathways[2]. As shown above, p53 has the tendency to promote Oxidative Phosphorylation and block glycolysis to oppose the Warburg phenomenon exhibited by cancer cells. The pentose phosphate pathway is promoted by p53 for cell survival purposes

In addition to the high rate of aerobic glycolysis, another major pathway of glucose metabolism called the Pentose Phosphate Pathway (PPP) is enhanced in tumor cells[47]. The PPP can contribute to the anabolic processes utilized for the growth of tumor cells by generating NADPH and ribose 5-phosphate from glucose catabolism, which are used as precursors for the biosynthesis of fatty acids and nucleotides respectively.

p53 plays a central role in controlling these pathways[48] by directly modulating tumor metabolism. It was recently demonstrated that tumor suppressor genes, in addition to their role in cell survival and apoptosis, play an important role in metabolic regulation and p53 was the first tumor suppressor categorized to regulate metabolism[49].

5.1.1 p53 and Oxidative Phosphorylation

Now that it has been established that a high glycolytic rate is important for the maintenance of tumors, it is safe to say that dampening the process of glycolysis hinders tumor development. p53 strives to perform this function by promoting OxPhos and blocking glycolysis.

p53 brings about the transcriptional activation of proteins such as the synthesis of cytochrome c oxidase 2 (SCO2) which is a key component in OxPhos. SCO2 in turn is required for the assembly of COX II subunit involved in the mitochondria electron transport chain. p53 also brings about posttranslational regulation of COX II subunit maintaining the stability and structural integrity of mitochondria. In addition, the apoptosis inducing factor (AIF), which is involved in maintenance of the mitochondrial integrity, is transcriptionally activated. p53 also exhibits certain intricate roles such as enhancing the rate of TCA cycle in order to promote mitochondrial respiration. Since p53 is directly involved in maintenance of the mitochondrial respiratory chain, it enhances mitochondrial oxidative phosphorylation in cells.

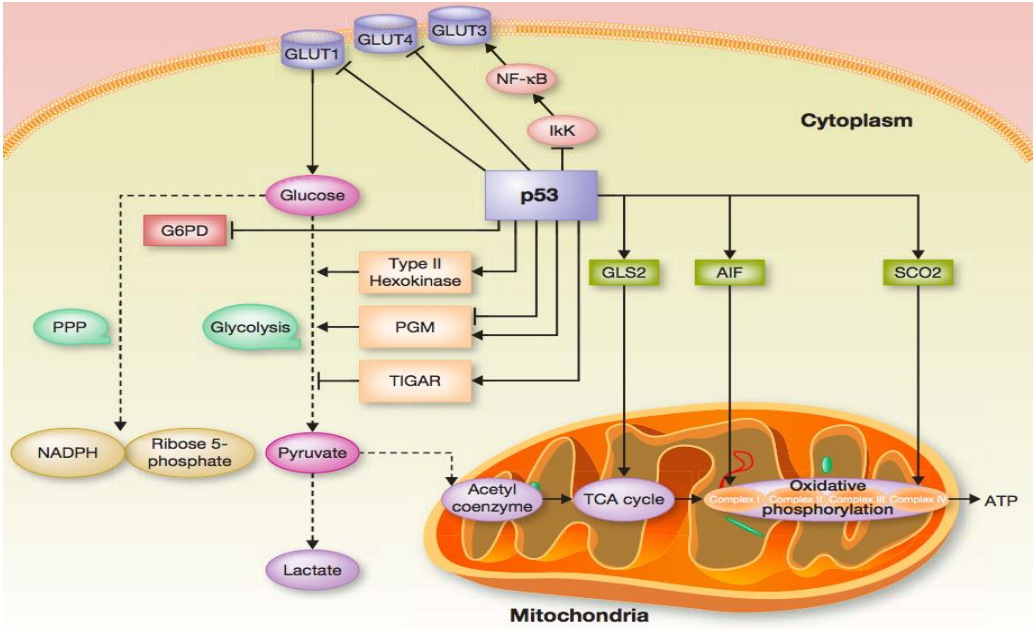

Fig. 5.2: p53 regulation of key factors and components involved in Oxidative Phosphorylation and glycolysis[49]

5.1.2 p53 and Glycolysis

p53 induces the expression of TIGAR by transcriptional activation and this in turn dephosphorylates fructose-2,6 biphosphate that is required for the activation of the enzyme 6-phosphofructo-1-kinase (PFK-1), crucial in glycolysis. PGM, phosphoglycerate mutase, is an enzyme involved in converting 3 phosphoglycerate to 2 phosphoglycerate during glycolysis and p53 acts by downregulating this enzyme through ubiquitination and inactivation. In addition to interfering with glycolytic enzymes, p53 can also reduce the intracellular level of glucose by inhibiting the expression of glucose transporters. This is achieved by the transcriptional repression of glucose transporters GLUT 1, GLUT 4 and an indirect repression of GLUT 3 expression by preventing the activation of the IKK-NF-kB pathway. With the sequence of these events, it is clear that p53 inhibits glycolysis while promoting OxPhos in cancer cells.

5.13 p53 and the pentose phosphate pathway

p53 also plays an important role in inhibiting the pentose phosphate pathway (PPP) utilized by cancer cells by suppressing the activity of glucose-6-phosphate dehydrogenase, a rate limiting enzyme of the PPP[49]. However, p53 can play a part in promoting the pentose phosphate pathway as well as shown in Fig. 5.1. This function isn't fully elucidated but is predicted to help cells survive moderate levels of stress encountered in normal conditions and provide energy for repair mechanisms[2]. These contradictory roles of p53 may be the reason why there is much uncertainty in this area and hopefully will display more clarity by fluorescent lifetime imaging microscopy (FLIM).

As previously discussed in chapter 1, upon stress, p53 has a dual role in either promoting the repair and survival of damaged cells or the permanent removal of these cells from the proliferating cycle by apoptosis. The different responses of p53 depend on the level of stress. It would be disastrous if cells underwent apoptosis every time they were even remotely stressed. Hence, it is safe to say that, the extent of damage influences the switch between cell repair and death.

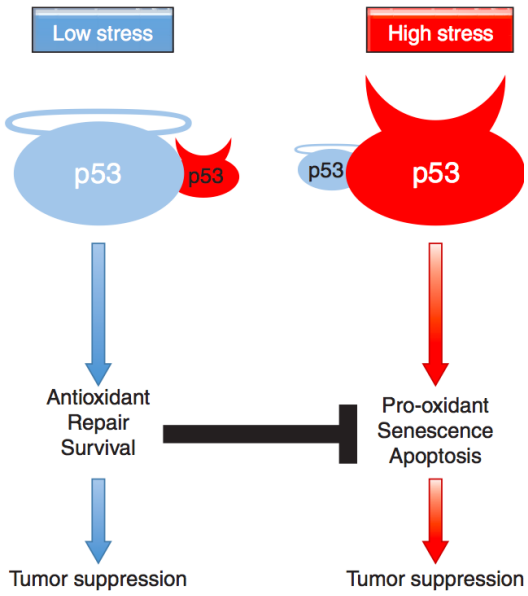

Fig. 5.3: p53 response depending on the extent of damage. When stress can be sustained, repair mechanisms are promoted whereas if the stress cannot be overcome contributing to significant damage, cells are not allowed to divide and are eventually destroyed[2]

To investigate whether the metabolic functions of p53 were influenced by the level of stress as well, fluorescent lifetime imaging microscopy (FLIM) was employed to detect changes in the metabolic pathways of the cell namely, oxidative phosphorylation.

5.2 Fluorescence Lifetime Imaging Microscopy

Fluorescence lifetime imaging microscopy is an imaging technique in cell biology that maps the lifetime of molecules within cells, tissues and whole organisms. Fluorescence lifetime is a measure of the time spent by the fluorophore in its excited state before returning to the ground state by emitting a small quantum of energy. It does not depend on the protein concentration and is characteristic of the type of molecule and its environment.

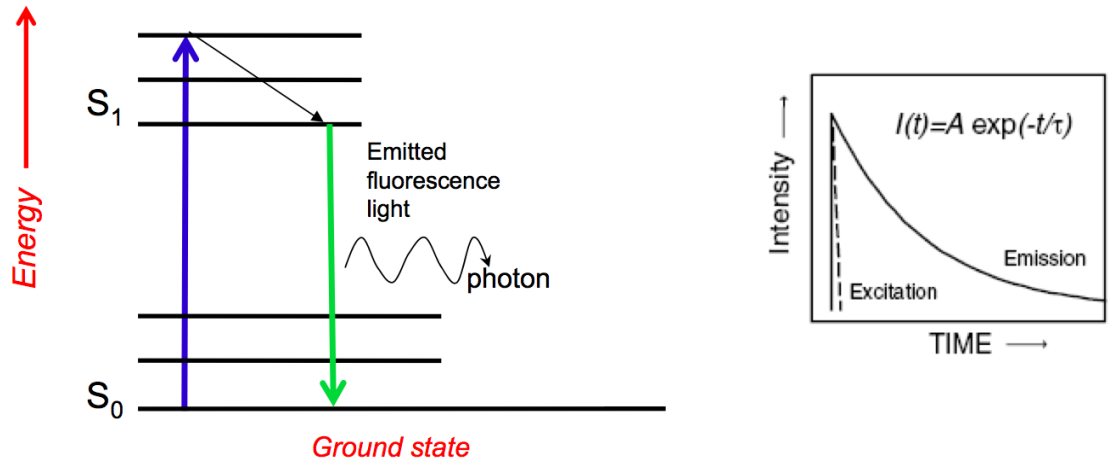

(a) (b)

Fig. 5.4 (a): Represents the decay of fluorophore from the excited state S1 to the ground state, S0; (b) Decay curve represented by the fluorescence intensity 'I' at time 't' where A is the initial fluorescence at t=0 and τ is the fluorescence lifetime

Every fluorescent chemical species has a characteristic lifetime and can be used for identification of the molecule in a sample. In an image, the decay of fluorescence is measured at every point generating 100,000-million possible decay courses that are impossible to decipher. By changing the data representation from the time delay histogram to a phasor approach, a global view of the

fluorescence decay at every pixel of an image can be provided[50]. The conversion of time domain to a frequency domain does not change any information but provides a simpler representation. Once the data is collected, a phasor transformation is applied to the data to get the coordinates, 'g' and 's', of the two dimensional phasor plot. The values of the g and s components are calculated by the sine-cosine transforms shown below:

$$g_i(\omega) = \int_0^\infty I(t)\cos(\omega t)dt \,/\, \int_0^\infty I(t)dt \qquad (10)$$

$$s_i(\omega) = \int_0^\infty I(t)\sin(\omega t)dt \,/\, \int_0^\infty I(t)dt \qquad (11)$$

where, I(t) is the decay at time t and ω is the angular repetition frequency of the laser

Each pixel of an image generates a point in the phasor plot and the phasor transformation is represented below:

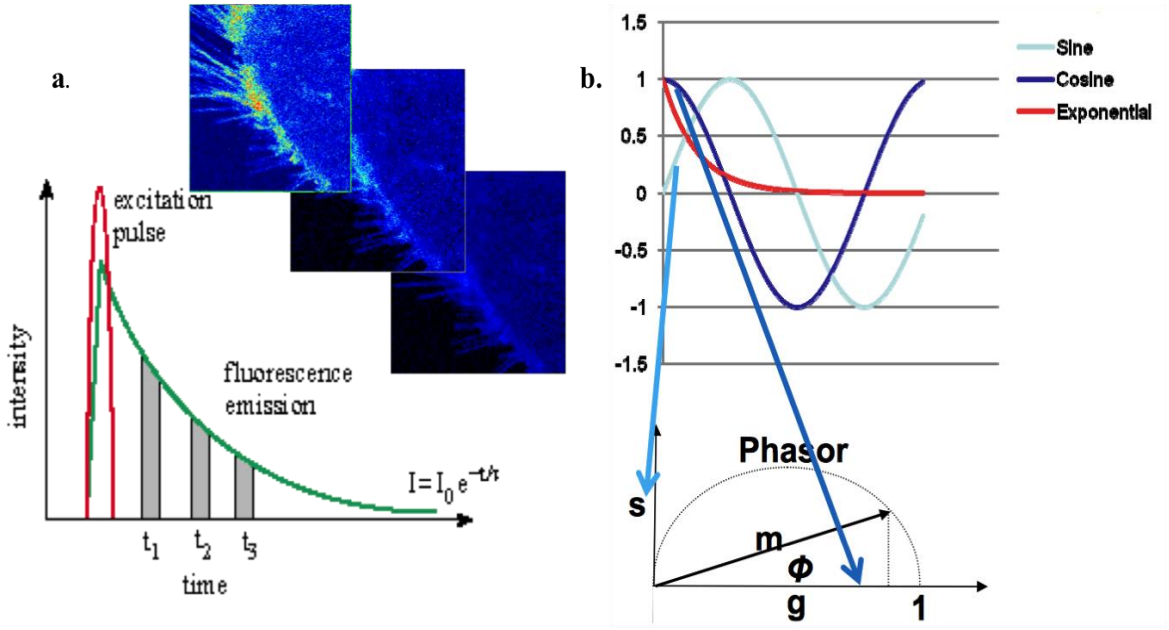

Fig. 5.5: (a) Histogram of time decay collected at every pixel (b) The decay curve is transformed to obtain the g and s coordinates of the phasor plot and is represented in red; the sine and cosine wave in the light blue and dark blue respectively; Φ is phase and m is the modulation of the signal

From the figure above, it is clear that a cosine transformation of a short decay corresponds to g=1 and a sine transformation of the same approaches s=0. A longer lifetime on the other hand would correspond to g=0 and s=1. Hence, depending on the lifetime of the species, it is plotted at different points within the universal circle in the phasor plot.

Multiple lifetime components arise from different molecular species or different conformations of the same molecule. Molecules exhibiting a single exponential decay will have their lifetimes plotted on the universal circle while multi exponential decays, follows the same algebra as vectors and will lie on a linear combination of their components. Since fluorescence lifetime is characteristic of a molecule, each molecular species has a specific phasor and can be identified based on their position in the phasor plot. For instance, by measuring the intrinsic lifetime of biomarkers such as NADH in living cells, information pertaining to cellular processes and interactions can be determined.

5.3 Lifetime of NADH

Nicotinamide adenine dinucleotide (NAD) is a coenzyme present in all living cells and is involved in redox reactions playing an important role in metabolism. It is the principal electron donor in glycolysis and electron acceptor in oxidative phosphorylation, hence existing in either its oxidized or reduced form[51]. The balance between the reduced and oxidized forms, NADH/NAD+ is known as the free to bound ratio[52]. This is an important component to determine the redox state of the cell that reflects the metabolic activity and health of these cells. A higher ratio value (↑NADH) is indicative of glycolytic reactions whereas a lower value (↑NAD+) favours Oxidative Phosphorylation.

NADH is autofluorescent and its fluorescence lifetime changes i.e. it has a shorter or longer lifetime component depending on whether it exists in its free or protein-bound state respectively. This feature can be exploited to obtain information about oxidation/reduction states in cells and enhance the understanding of cellular processes. By achieving this, the metabolic role of p53 in cells can be investigated at different time points and conditions.

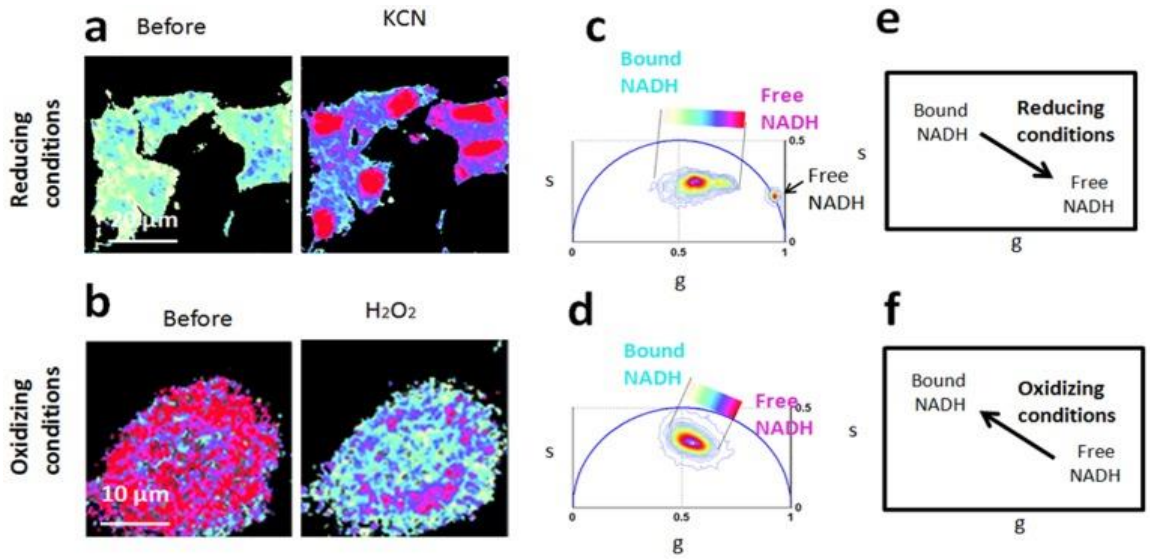

Fig. 5.6: Experiments were conducted by Stringari et al[53] to observe the shifts in the NADH metabolic trajectory. (a)Potassium Cyanide was added to block cellular respiration and induce a glycolytic environment where the trajectory shifts towards free NADH. (b) In another experiment, hydrogen peroxide was added to induce oxidative stress and shift the phasor signature towards the bound state.

However, the issue of whether FLIM may permit separation of NADH and NADPH fluorescence is yet to be addressed[54]. NADP exists in its reduced and oxidized state as well, and is a cofactor involved in anabolic reactions such as nucleic acid and lipid synthesis. The phosphate pentose pathway is the major source of NADPH and its significance in metabolism will be explained further in the discussion.

The phasor FLIM signature corresponds to the typical multiexponential lifetime distribution at the center of the phasor plot and similar to the figure above, an interpretation of this phasor distribution can provide crucial information of the state of the cells.

5.4 Materials and Methods

The primary cell culture, plasmids and the reagents (cisplatin) employed are the same as described in the previous chapter. Mouse Embryonic fibroblast (MEF) cells with p53 knock out was provided by the Edinger lab (University of California, Irvine) and used as a control in all the experiments. The culture media and protocol for passaging these cells were similar to those employed for the NIH3T3 cells.

5.4.1 Microscope set-up

Two photon-excitation fluorescence measurements were taken on the Zeiss LSM 710 confocal microscope coupled with a Mai Tai Ti:Sapphire laser set to 740 nm for NADH. The FLIM data is acquired with the Fast FLIM system (FLIMbox) by ISS (Champaign, IL). 40 frames were integrated per FLIM dataset in order to collect enough photon counts at a pixel dwell time of 25.21µs and a frame size of 256x256. An electronic zoom of 2.5-3 was used to capture the entire cell while a zoom of 12 was used to focus only on the nuclei of the cells. Two channels were used to collect the emission light; 417/60nm filter for NADH and a 5120/90 nm filter for direct EGFP detection. The phasor plot was calibrated using Coumarin-6 and rhodamine 110 that have single exponential lifetimes of 2.50 ns and 4.00 respectively.

Fig. 5.7: Fast FLIM system (ISS) with a digital frequency domain (DFD) approach and equipped with standard light detectors

5.4.2 Data Analysis

The SIM FCS software was employed for the FLIM analysis as well. The fraction of free and bound NADH in the cells can easily be determined by selection of its position in the phasor plot. Individual calls were masked to obtain a region of interest and determine their ‘g’ and ‘s’ coordinates.

5.5 Results

The FLIM analysis of NIH3T3 cells expressing p53-GFP stimulated with cisplatin is shown below. The nucleus in general, exhibits more free NADH compared to the rest of the cytoplasm as denoted by the pink pixels. The cells start off with a long lifetime and with each time point shift to a shorter lifetime (white → pink). At 300 minutes, it reverts to a position in the phasor plot corresponding to a long lifetime component. The phasor plot shows the metabolic trajectory of bound and free NADH.

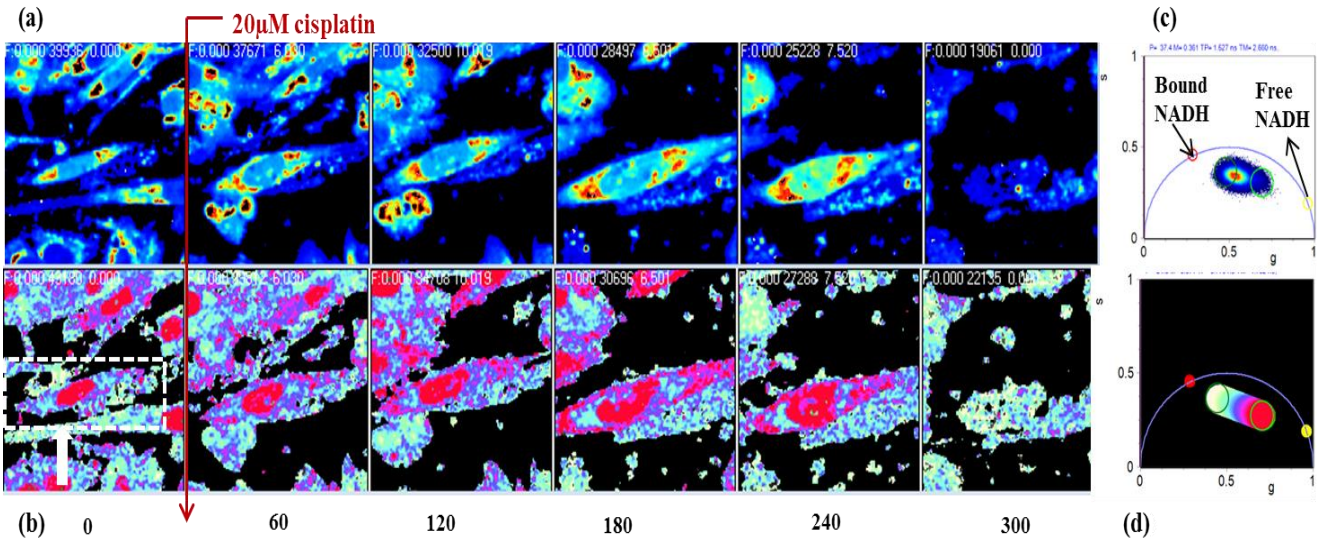

Fig. 5.8: FLIM analysis of NIH3t3 cells expressing p53-GFP post DNA damage (a) Intensity map of the same cell as a function of time (b) Distribution of free to bound NADH ratio in the cell with time (c) Phasor plot showing the shift of lifetime from a bound state to free state with each time point (d) Map of colour points for representation of bound and free NADH, denoted by white and pink respectively. The red and yellow points represent the bound and free NADH lifetimes at 3.20 and 0.4 ns respectively.

The shift in lifetime observed above follows a trend in most NIH3T3 cells and is represented more clearly in the figure below.

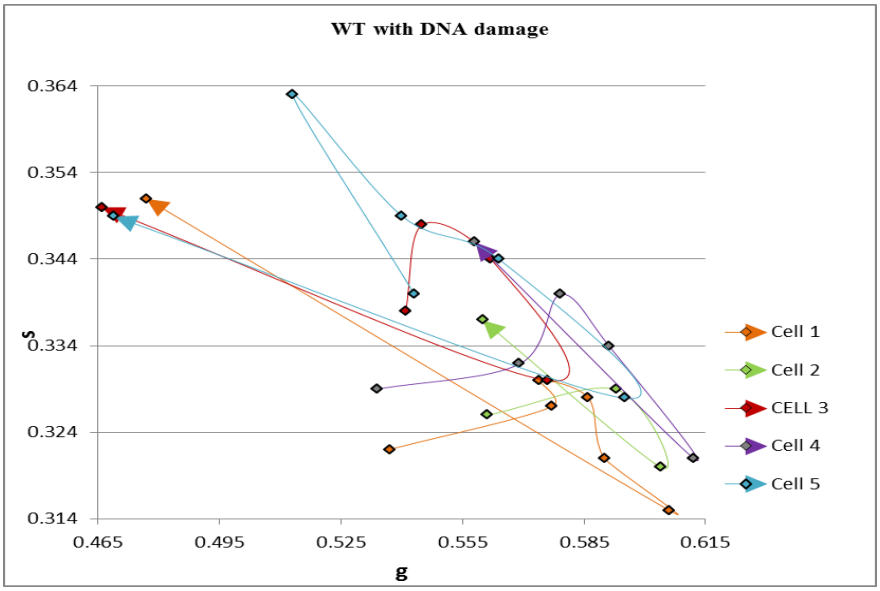

Fig 5.9: The 'g' and 's' coordinates of NIH3t3 cells transfected with p53-GFP at each time point of 60 minute intervals before and after DNA damage. The arrow indicates the direction of the trajectory at the last time point (300mins) and as seen each cell follows a similar trajectory.

Similar experiments and analysis were carried out with different conditions that serve as controls to determine the significance of the shift observed above.

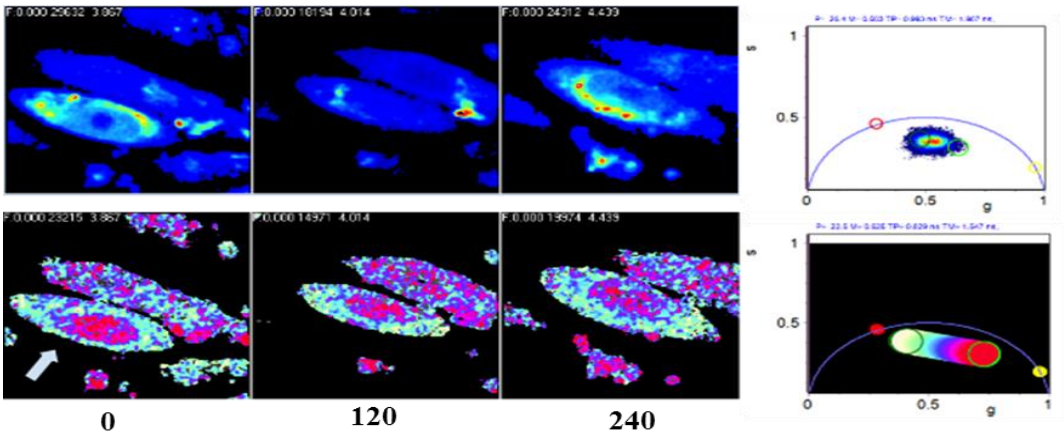

Fig. 5.10: FLIM analysis of NIH3T3 cells transfected with p53-GFP **without** DNA damage. The same cell was tracked for a period of four hours to observe the presence of any significant shift in lifetime.

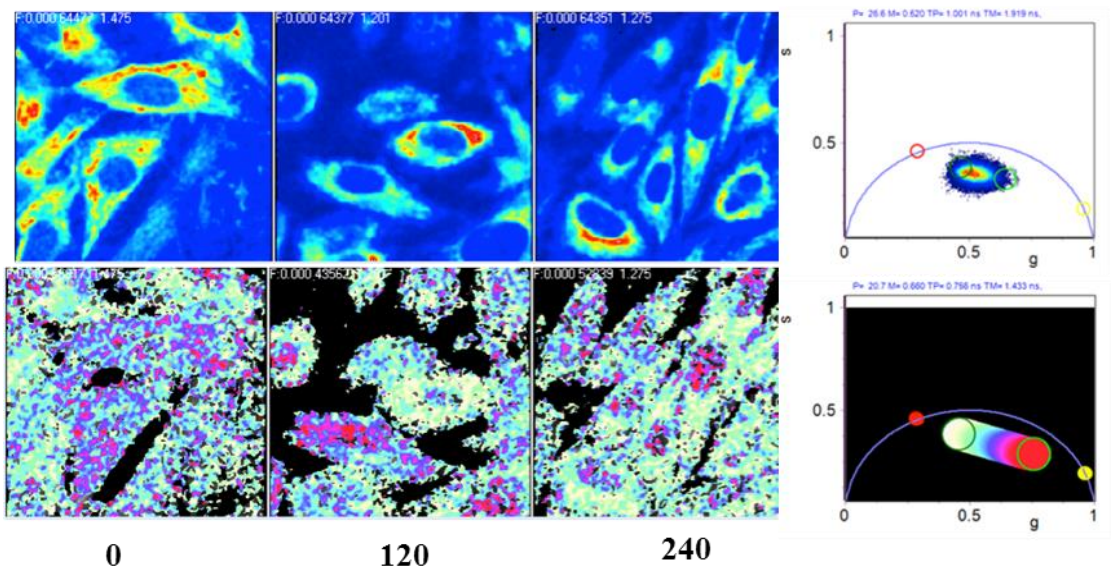

Fig. 5.11: FLIM analysis of NIH3T3 cells exhibiting no transfection and no DNA damage. They serve as a negative control and do not exhibit any substantial shift in the lifetime, mainly comprising of a more bound NADH state denoted by the majority of white pixels.

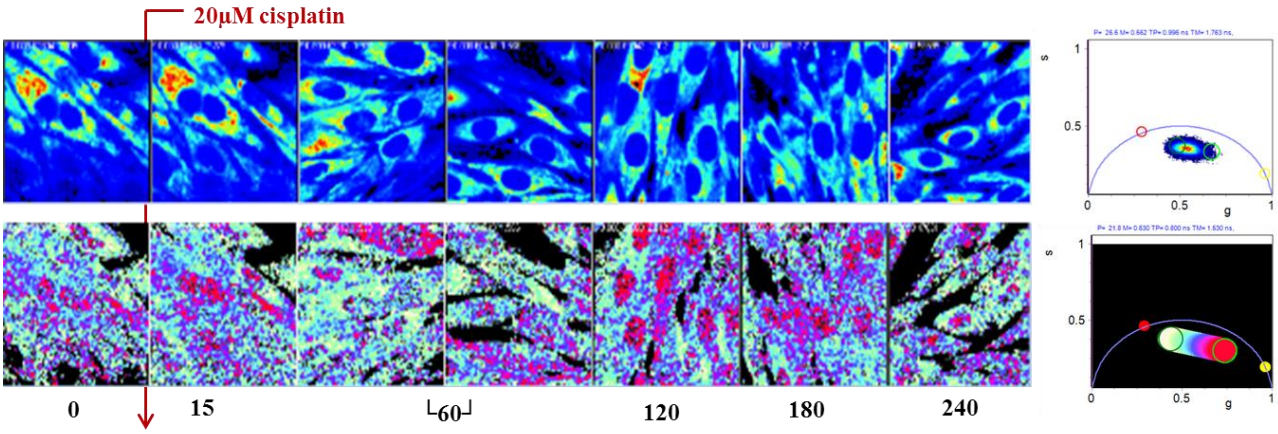

Fig. 5.12: FLIM analysis of non-transfected NIH3T3 cells **with** DNA damage. The lifetime shift is significantly more compared to the non-transfected cells without DNA damage but do not exhibit the same trend as damaged cells expressing p53-GFP

To fully elucidate the contribution of p53-GFP in the lifetime shifts, the experiment was repeated in p53 knock out mouse embryonic fibroblasts. A shift to a relatively free state is observed at a time point of 240 minutes as observed in the phasor plot and images below.

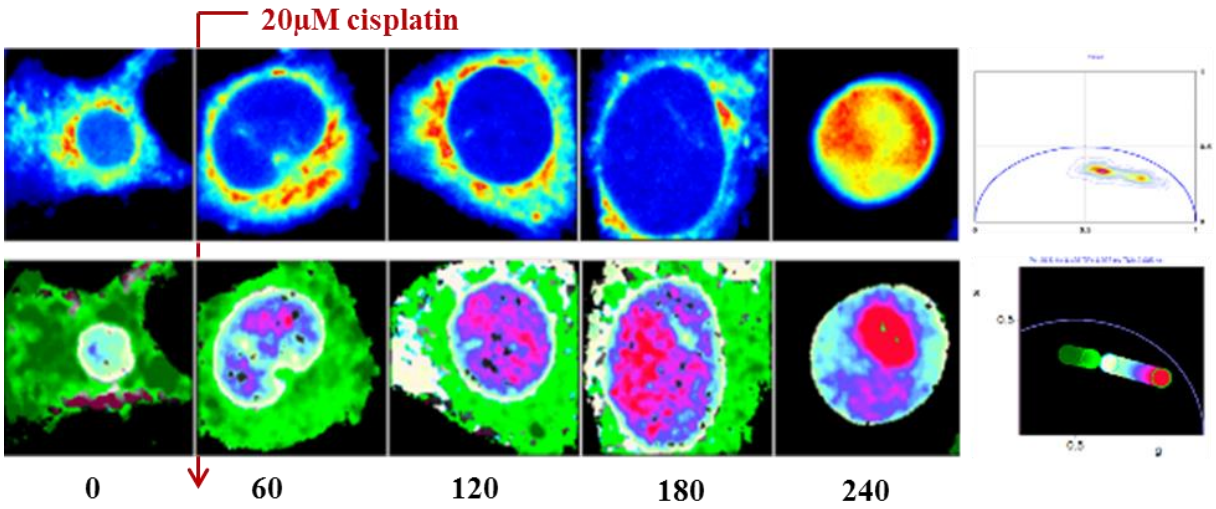

Fig. 5.13: FLIM analysis of p53 KO MEF cells upon DNA damage with respect to time

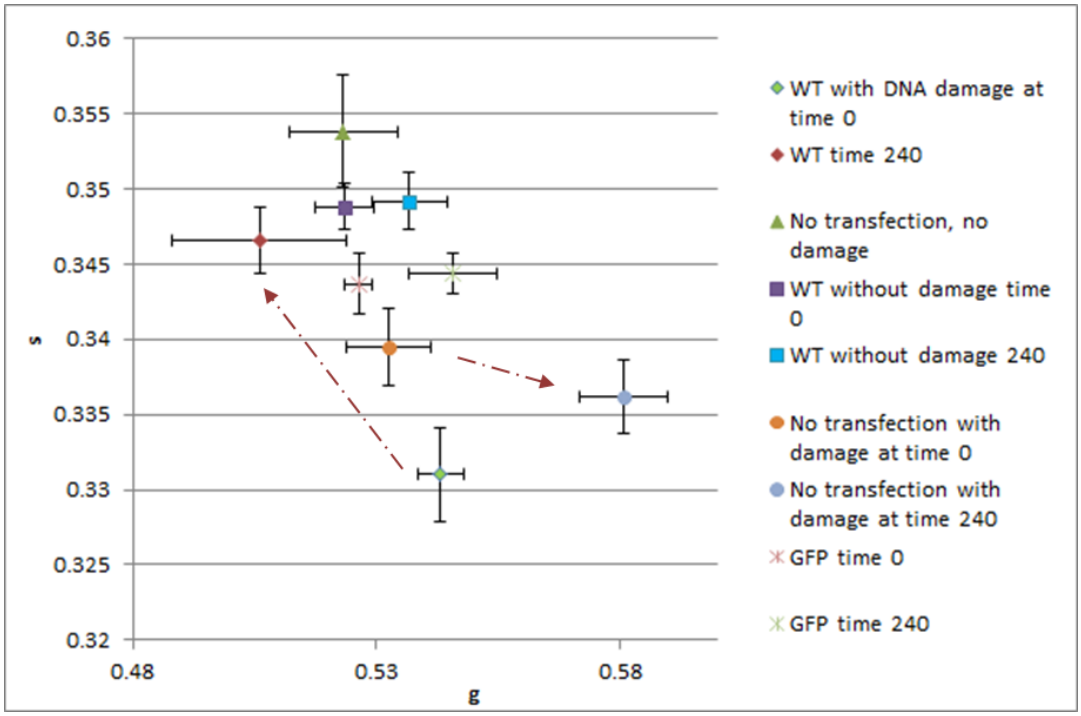

Fig 5.14: Cluster of 'g' and 's' coordinates corresponding to the positions in the phasor plot of NIH3T3 cells exhibiting various conditions. Noted time is in minutes.

5.6 Discussion

It is observed as seen in fig. 5.8, that in the cells expressing p53-GFP and damaged with cisplatin, the metabolic trajectory of NADH goes from a bound to a free state gradually and then reverts to a bound state when the cell undergoes apoptosis. The time scale of this transition differs from cell to cell depending on the extent of expression of the plasmid but they tend to follow the same trend in the 4 hour time period as shown in fig. 5.9. This was especially observed in almost all cells undergoing apoptosis while the cells that were relatively healthier were characterized by the lifetime of NADH in the free state. A number of different experimental conditions were employed to better understand the significance of the metabolic trajectory and a plot of the lifetimes of each experimental condition is shown in fig. 5.13. The same trajectory isn't observed in the non-transfected cells damaged with cisplatin as seen in fig. 5.12 and even though they possess endogenous levels of p53, the time scale of observation was probably insufficient to capture any such response. These cells also look healthier compared to the cells with p53-GFP at the same time points despite DNA damage. The non-transfected cells without DNA damage serves as a good control while the comparison of the effects of DNA damage on the non-transfected cells and cells expressing p53-GFP give an account of the p53 contribution in the metabolic trajectory. The lifetime of cells expressing p53-GFP without any DNA damage was measured as well to assess whether transfection and/or the stress of laser exposure had any impact on the metabolic shift. The lifetimes at time 0 and 240 are more or less in the same position with a very slight shift as seen in the fig. 5.10 and fig. 5.13. Indicated by the red arrows in fig 5.13, the p53-gfp cells shift to a more bound state than they start off with while the non-transfected cells shift to a more free state. The lifetime of cells expressing GFP alone is also

plotted for the same time scale of DNA damage to demonstrate that GFP displays no such effect and p53 is responsible for this shift.

The p53 KO cells, do not exhibit any such property either as seen in fig. 5.14, thereby making it easy to assume this phenomenon as an attribute of p53. In fact, in these cells, the shift to a more free NADH is encountered and since they have absolutely no p53, it can be assumed that aerobic glycolysis or in other words, the Warburg effect is in play promoting these cells to adopt a cancerous phenotype. On the other hand, the change in the conformation of the cell is hard to decipher and may also be undergoing apoptosis by a non p53 dependent mechanism. Now the question is, why does p53 induce this sudden jump in the trajectory? Moreover, if p53 is well known to inhibit glycolysis, the initial shift from a bound to a free state seems inconsistent with the literature. However, a thorough understanding of the different metabolic pathways may provide a reasonable explanation.

As mentioned in the introduction, p53 has conflicting roles in inhibiting and promoting the pentose phosphate pathway.

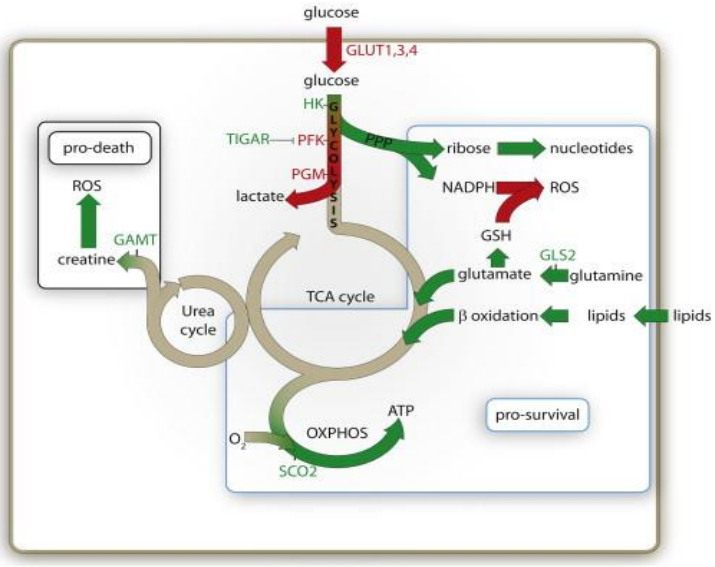

Fig. 5.15: Overview of the metabolic functions of p53. Green arrows indicate p53 promotion while the red arrows indicate the inhibition[55].

Perhaps, the two seemingly contradictory effects of p53 on the PPP could be explained by its two activities; namely, as an inducer of cell cycle arrest and/or apoptosis.

In response to DNA damage, p53-mediated cell cycle arrest enables the cells to repair the damage before re-entering the cell cycle. Under these conditions, the positive effect of p53 on the PPP, as seen in fig. 5.14, maintains cell survival while generating nucleotides for DNA repair. If the cells are unable to repair the damage, p53 activation induces cell death. Under these conditions, inhibition of the PPP by p53 accelerates cell death by decreasing NADPH levels and consequently increasing intracellular levels of ROS[56].

In the case of the cells damaged with cisplatin, the trajectory tends to shift towards a more free state, representing the NAD(P)H lifetime instead, which could be indicative of the PPP for cell repair. Although, due to high extent of damage, these cells become irreparable and to prevent the proliferation of damaged cells, p53 redirects it to a state of bound NADH, bringing about apoptosis by some unknown mechanism. The mechanism of apoptosis is unclear but the pro-oxidant function of p53 is assumed to promote oxidative stress by increasing the reactive oxygen species level (ROS) and kill the cells[2]. The corresponding lifetime could be representative of the metabolic trajectory for oxidized lipids[57] but is still under investigation and should be explored further.

Metabolism is affected by a number of factors such as pH, glucose level, availability of CO2 etc. making it difficult to comprehend the results with accuracy as there may be discrepancies in the data. In depth examination is required to fully elucidate the exact pathway of metabolism adapted by cells as a stress response. This field of study holds promising results and additional experimentation should be employed to observe the shifts in metabolism brought about by p53 in

cancer cells. In the future, I'm certain that further research will uncover in detail the metabolic pathway and role of p53 in its anticancer function.

5.7 Conclusion

Cancer is a complex disease with numerous genetic and epigenetic alterations[58]. Despite the continuous progress in the field of cancer therapy, there is no sure cure developed as yet. Due to the critical role of p53 in cancer, ample research has been carried out to understand its mechanism of action. Targeting of this protein for drug development has become widely popular and in addition to restoring its wild type function in tumors, drugs that mimic the metabolic effect of p53 are being developed. These drugs are able to perturb the cancer cell metabolism and inhibit their proliferation[49]. p53 plays an important inhibitory role in inhibiting the metabolic reprogramming of cancer cells and the p53 pathway components that are involved in this aspect of p53 function should therefore be considered as novel targets for tumor therapy.

In conclusion, I would like to say that the study of p53 regulation has been immensely insightful in the field of tumor suppression. With the number of opportunities p53 provides us in our fight against cancer; it is simply a matter of time that it will cease to be a 'deadly disease to humankind'.

BIBLIOGRAPHY

1. Strachan, T. & Read, A. P. *Human molecular genetics 2*. (1999).

2. Gottlieb, E. & Vousden, K. H. P53 Regulation of Metabolic Pathways. *Cold Spring Harb. Perspect. Biol.* **2,** (2010).

3. Wei, C. L. *et al.* A global map of p53 transcription-factor binding sites in the human genome. *Cell* **124,** 207–219 (2006).

4. Lorne J. HofsethNewton, A. C., S. Perwez Hussain & Curtis C. Harris. p53: 25 years after its discovery. *Trends Pharmacol. Sci.* **25,** 177–81 (2004).

5. Joerger, A. C. & Fersht, A. R. The tumor suppressor p53: from structures to drug discovery. *Cold Spring Harb. Perspect. Biol.* **2,** 1–20 (2010).

6. Weinberg, R. L., Veprintsev, D. B. & Fersht, A. R. Cooperative binding of tetrameric p53 to DNA. *J. Mol. Biol.* **341,** 1145–1159 (2004).

7. McLure, K. G. & Lee, P. W. K. How p53 binds DNA as a tetramer. *EMBO J.* **17,** 3342–3350 (1998).

8. Moll, U. M. & Petrenko, O. The MDM2-p53 interaction. *Mol. Cancer Res.* **1,** 1001–1008 (2003).

9. Barak, Y., Gottlieb, E., Juven-Gershon, T. & Oren, M. Regulation of mdm2 expression by p53: Alternative promoters produce transcripts with nonidentical translation potential. *Genes Dev.* **8,** 1739–1749 (1994).

10. Brady, C. a & Attardi, L. D. P53 At a Glance. *J. Cell Sci.* **123,** 2527–2532 (2010).

11. Waterman, J. L., Shenk, J. L. & Halazonetis, T. D. The dihedral symmetry of the p53 tetramerization domain mandates a conformational switch upon DNA binding. *EMBO J.* **14,** 512–519 (1995).

12. Chène, P. Inhibiting the p53-MDM2 interaction: an important target for cancer therapy. *Nat. Rev. Cancer* **3,** 102–109 (2003).

13. Bell, S., Klein, C., Müller, L., Hansen, S. & Buchner, J. p53 contains large unstructured regions in its native state. *J. Mol. Biol.* **322,** 917–927 (2002).

14. Xu, J. *et al.* Gain of function of mutant p53 by coaggregation with multiple tumor suppressors. *Nat. Chem. Biol.* **7,** 285–295 (2011).

15. Freed-pastor, W. a & Prives, C. Mutant p53 : one name , many proteins Mutant p53 : one name , many proteins. 1268–1286 (2012). doi:10.1101/gad.190678.112

16. Van Oijen, M. G. C. T. & Slootweg, P. J. Gain-of-function mutations in the tumor suppressor gene p53. *Clinical Cancer Research* **6,** 2138–2145 (2000).

17. Yu, X., Vazquez, A., Levine, A. J. & Carpizo, D. R. Allele-Specific p53 Mutant Reactivation. *Cancer Cell* **21,** 614–625 (2012).

18. Muller, P. a J. & Vousden, K. H. P53 Mutations in Cancer. *Nat. Cell Biol.* **15,** 2–8 (2013).

19. Chène, P. The role of tetramerization in p53 function. *Oncogene* **20,** 2611–2617 (2001).

20. Davison, T. S., Yin, P., Nie, E., Kay, C. & Arrowsmith, C. H. Characterization of the oligomerization defects of two p53 mutants found in families with Li-Fraumeni and Li-Fraumeni-like syndrome. *Oncogene* **17,** 651–656 (1998).

21. Wassman, C. D. *et al.* Computational identification of a transiently open L1/S3 pocket for reactivation of mutant p53. *Nat. Commun.* **4,** 1407 (2013).

22. Digman, M. a, Dalal, R., Horwitz, A. F. & Gratton, E. Mapping the number of molecules and brightness in the laser scanning microscope. *Biophys. J.* **94,** 2320–2332 (2008).

23. Grollman, A. P. Inhibitors of protein biosynthesis. II. Mode of action of anisomycin. *J. Biol. Chem.* **242,** 3226–3233 (1967).

24. Dasari, S. & Bernard Tchounwou, P. Cisplatin in Cancer therapy: Molecular mechanisms of action. *Eur. J. Pharmacol.* **740,** 364–378 (2014).

25. Roos, W. P. & Kaina, B. DNA damage-induced cell death by apoptosis. *Trends in Molecular Medicine* **12,** 440–450 (2006).

26. Anderson, C. W. & Appella, E. in *Handbook of Cell Signaling, 2/e* **3,** 2185–2204 (2010).

27. Kishi, H. *et al.* Osmotic Shock Induces G1 Arrest through p53 Phosphorylation at Ser33 by Activated p38MAPK without Phosphorylation at Ser15 and Ser20. *J. Biol. Chem.* **276,** 39115–39122 (2001).

28. Levine, A. J. & Oren, M. The first 30 years of p53: growing ever more complex. *Nat. Rev. Cancer* **9,** 749–758 (2009).

29. Wolf, D. & Rotter, V. Inactivation of p53 gene expression by an insertion of Moloney murine leukemia virus-like DNA sequences. *Mol. Cell. Biol.* **4,** 1402–1410 (1984).

30. Eliyahu, D. *et al.* Meth A fibrosarcoma cells express two transforming mutant p53 species. *Oncogene* **3,** 313–321 (1988).

31. Baker, S. J. *et al.* Chromosome 17 deletions and p53 gene mutations in colorectal carcinomas. *Science* **244,** 217–221 (1989).

32. Eliyahu, D., Michalovitz, D., Eliyahu, S., Pinhasi-Kimhi, O. & Oren, M. Wild-type p53 can inhibit oncogene-mediated focus formation. *Proc. Natl. Acad. Sci. U. S. A.* **86,** 8763–8767 (1989).

33. Weinert, T. DNA Damage and Checkpoint Pathways. *Cell* **94,** 555–558 (1998).

34. Kastan, M. B., Onyekwere, O., Sidransky, D., Vogelstein, B. & Craig, R. W. Participation of p53 protein in the cellular response to DNA damage. *Cancer Res.* **51,** 6304–6311 (1991).

35. Kastan, M. B. *et al.* A mammalian cell cycle checkpoint pathway utilizing p53 and GADD45 is defective in ataxia-telangiectasia. *Cell* **71,** 587–597 (1992).

36. Stewart, N., Hicks, G. G., Paraskevas, F. & Mowat, M. Evidence for a second cell cycle block at G2/M by p53. *Oncogene* **10,** 109–115 (1995).

37. Yonish-Rouach, E. *et al.* Wild-type p53 induces apoptosis of myeloid leukaemic cells that is inhibited by interleukin-6. *Nature* **352,** 345–347 (1991).

38. Shaw, P. *et al.* Induction of apoptosis by wild-type p53 in a human colon tumor-derived cell line. *Proc. Natl. Acad. Sci. U. S. A.* **89,** 4495–4499 (1992).

39. Palmer, A. G. & Thompson, N. L. Molecular aggregation characterized by high order autocorrelation in fluorescence correlation spectroscopy. *Biophys. J.* **52,** 257–270 (1987).

40. Hillesheim, L. N. & Müller, J. D. The photon counting histogram in fluorescence fluctuation spectroscopy with non-ideal photodetectors. *Biophys. J.* **85,** 1948–1958 (2003).

41. Cubells, M. P., Aixela, J. P., Brumos, V. G., Pou, S. D. & Flaque, M. V. Stability of cisplatin in sodium chloride 0.9% intravenous solution related to the container's material. *Pharm. World Sci.* **15,** 34–36 (1993).

42. Selivanova, G. & Wiman, K. G. Reactivation of mutant p53: molecular mechanisms and therapeutic potential. *Oncogene* **26,** 2243–2254 (2007).

43. Martinez, J. D. Restoring p53 tumor suppressor activity as an anticancer therapeutic strategy. *Futur. Oncol.* **6,** 1857–1862 (2010).

44. Xue, W. *et al.* Senescence and tumour clearance is triggered by p53 restoration in murine liver carcinomas. *Nature* **445,** 656–660 (2007).

45. Yu, X., Narayanan, S., Vazquez, A. & Carpizo, D. R. Small molecule compounds targeting the p53 pathway: Are we finally making progress? *Apoptosis* **19,** 1055–1068 (2014).

46. BURK, D. & SCHADE, A. L. On respiratory impairment in cancer cells. *Science* **124,** 270–272 (1956).

47. Jiang, P. *et al.* p53 regulates biosynthesis through direct inactivation of glucose-6-phosphate dehydrogenase. *Nat. Cell Biol.* **13,** 310–316 (2011).

48. Vousden, K. H. & Prives, C. Blinded by the Light: The Growing Complexity of p53. *Cell* **137,** 413–431 (2009).

49. Shen, L. *et al.* The fundamental role of the p53 pathway in tumor metabolism and its implication in tumor therapy. *Clin. Cancer Res.* **18,** 1561–1567 (2012).

50. Digman, M. A., Caiolfa, V. R., Zamai, M. & Gratton, E. The phasor approach to fluorescence lifetime imaging analysis. *Biophysical journal* **94,** L14–L16 (2008).

51. Skala, M. C. *et al.* In vivo multiphoton microscopy of NADH and FAD redox states, fluorescence lifetimes, and cellular morphology in precancerous epithelia. *Proc. Natl. Acad. Sci. U. S. A.* **104,** 19494–19499 (2007).

52. Stringari, C. *et al.* In Vivo Single-Cell Detection of Metabolic Oscillations in Stem Cells. *Cell Rep.* **10,** 1–7 (2015).

53. Stringari, C., Nourse, J. L., Flanagan, L. A. & Gratton, E. Phasor Fluorescence Lifetime Microscopy of Free and Protein-Bound NADH Reveals Neural Stem Cell Differentiation Potential. *PLoS One* **7,** (2012).

54. Blacker, T. S. *et al.* Separating NADH and NADPH fluorescence in live cells and tissues using FLIM. *Nat. Commun.* **5,** 3936 (2014).

55. Frezza, C. & Martins, C. P. From tumor prevention to therapy: Empowering p53 to fight back. *Drug Resist. Updat.* **15,** 258–267 (2012).

56. Patra, K. C. & Hay, N. The pentose phosphate pathway and cancer. *Trends in Biochemical Sciences* **39,** 347–354 (2014).

57. Datta, R., Alfonso-García, A., Cinco, R. & Gratton, E. Fluorescence lifetime imaging of endogenous biomarker of oxidative stress. *Sci. Rep.* **5,** 9848 (2015).

58. Wang, Z. & Sun, Y. Targeting p53 for Novel Anticancer Therapy. *Transl. Oncol.* **3,** 1–12 (2010).